Journal of Building Engineering 43 (2021) 103171

Contents lists available at ScienceDirect

Journal of Building Engineering

journal homepage: www.elsevier.com/locate/jobe

Effects of multiscale carbon-based conductive fillers on the performances of a self-sensing cementitious geocomposite

Mohammadmahdi Abedi [a], Raul Fangueiro [b,c,*], António Gomes Correia [a]

[a] Department of Civil Engineering, ISISE, University of Minho, Campus de Azurém, 4800-058, Guimarães, Portugal
[b] Department of Mechanical Engineering, University of Minho, Campus de Azurém, 4800-058, Guimarães, Portugal
[c] Centre for Textile Science and Technology, School of Engineering, University of Minho, Guimarães, Portugal

ARTICLE INFO

Keywords:
Cementitious stabilised sand: graphene: carbon nanotubes: self-sensing: multiscale

ABSTRACT

In this study, the effects of multiscale conductive carbon fillers, including carbon nanotubes (CNTs), graphene nanoplatelets (GNPs), and carbon fibres (CFs), on the mechanical and microstructural properties, durability, and piezoresistivity of cementitious stabilised sand (CSS) were investigated. In this route, the surface of the CFs was modified via an oxidation process to improve their interfacial performance and dispersion. An optimum amount of hybrid CNT/GNP with different concentrations of CFs was incorporated into the CSS, and specimens were fabricated using the standard compaction method at the optimum water content. The interfacial properties of the CFs were studied by performing pullout tests and several chemical analyses. The variations in the mechanical and microstructural, durability, and piezoresistivity of the CSS, were investigated by various tests. In addition, the status of the specimens in terms of residual strain and damages was identified by the digital image correlation technique. The results showed a considerable improvement in the interfacial properties of the modified CFs in terms of physical and chemical bonding with the cement matrix. In addition, a combination of 0.17% CNT/GNP (1:1, by weight of dry sand) with 0.75% CF can improve the maximum dry density and mechanical properties, as well as the ductility and durability of the CSS. In addition, using multiscale conductive fillers resulted in a considerable enhancement in the electrical conductivity and piezoresistivity of the CSS. The outcomes indicate the immense potential of CNT/GNP/CF for the development of a sustainable self-sensing cementitious geocomposite.

1. Introduction

Cementitious stabilised sand (CSS) is one of the most conventional and economical cementitious geocomposites and is widely used in various civil infrastructures such as structural foundations, roads, railways, bridges, and tunnels [1,2]. However, cementitious composites are generally vulnerable to damage and degradation over time. The deterioration and breakdown of cementitious composites are primarily caused by inherent defects, material ageing, aggressive environmental effects, overloading, prolonged utilisation and duty cycles, and a lack of adequate inspection and maintenance [3,4]. These factors weaken the composites and enable the extension of nanoscale cracks to microcracks between the microstructures over time and consequently, result in the sudden collapse of the structures. However, the timely detection of such damages and proper maintenance can significantly enhance the service life of structures and prevent sudden failures [5,6]. Self-sensing or self-diagnosing cementitious composites are multifunctional composites that have the ability to sense their own conditions, such as stress, strain, damage, and temperature [3,7]. In contrast to most infrastructure monitoring methods, such as those using strain gauges, fibre optics, and shape memory alloys, which involve a limited number of sensors distributed over large areas of infrastructure, self-sensing composites with intrinsic sensing capabilities based on piezoresistivity provide a more integrated, real-time, and practical solution for infrastructural damage detection by considering the properties and nature of the geomaterial [8,9]. Indeed, self-sensing infrastructures, in addition to the early detection of damages, can gain the required information for instrumentation and smart urban management, such as transportation. Self-sensing composites are generally fabricated by the dispersion of a conductive phase in a cement matrix [10,11]. These conductive fillers create several random conductive paths in the cementitious phase based on percolation and electron quantum tunnelling effects, and their

* Corresponding author. Department of Mechanical Engineering, University of Minho, Campus de Azurém, 4800-058, Guimarães, Portugal.
E-mail address: rfangueiro@dem.uminho.pt (R. Fangueiro).

https://doi.org/10.1016/j.jobe.2021.103171
Received 25 June 2021; Received in revised form 19 August 2021; Accepted 20 August 2021
Available online 2 September 2021

electrical resistivity is affected by external factors such as stress, strain, and temperature. Indeed, the effects of external factors on cementitious composites can be detected by measuring the fractional change in electrical resistivity [3]. However, the sensitivity and performance of self-sensing composites are affected by numerous factors including electrode status, current, temperature, humidity, and loading [12]. Among these factors, the type of conductive phase and their concentration and distribution are particularly important [10,13–20]. Although various types of fibrous materials and nanomaterials have been used as the conductive phase in cementitious matrices, carbon-based materials such as carbon short fibres (CFs), carbon nanotubes (CNTs), and graphene nanoplatelets (GNPs) have attracted increasing attention owing to their unique electrical, physical, and mechanical properties [8,21]. Furthermore, the incorporation of a certain amount of these carbon materials into cementitious composites can enhance their mechanical and microstructural properties and durability by bridging and/or deviating cracks, increasing the cement hydration rate, and improving their filler function mechanism [22–27]. Nevertheless, the percolation threshold of self-sensing cementitious composites with adequate sensitivity is much higher than the concentration required for improving the physical and mechanical performance, which increases the cost of production and agglomerate formation [8]. Recent studies on the hybrid or multiple applications of these conductive fillers have demonstrated their common co-effects [8,18,28–31].

In this study, a triple combination of CNT, GNP, and CF was used to develop a self-sensing cementitious geocomposite, which is an original material design to the best of our knowledge. The combination of different conductive fillers with 1D and 2D geometrical shapes at the micro-and nanoscale can enhance the percolation and electron quantum tunnelling effects and decrease the percolation threshold significantly [8,28]. The presence of CNTs and GNPs increases the sensitivity of the composite by the formation of several nanoscale conductive paths, owing to their high specific surface area and aspect ratio [10,32,33]. In contrast, the CFs increase the measurable range of the composite by generating micro-scale conductive paths [9,32]. In addition, the low ductility of cementitious composites which is also affected by CNTs in some cases, can be compensated by the CFs [34–39]. Furthermore, it is expected that the piezoresistivity of the composite will not decrease sharply upon exposure to destructive environmental factors and the possible chemical corrosion of carbon nanomaterials (CNMs) over time. Moreover, the triple combination of CNT/GNP/CF can fill a broader range of porosities in the cementitious matrix in addition to bridging cracks at different scales. Therefore, in this study, different concentrations of modified CFs were incorporated into a cementitious composite containing hybrid CNT/GNP to develop a sustainable self-sensing cementitious composite with high physical, mechanical, and piezoresistive performance. The effects of these combinations on the maximum dry density and degree of saturation were evaluated, and the specimens were fabricated by a standard compaction method (ASTM D698). Furthermore, the surficial properties of the modified CFs were studied by performing pullout tests and several chemical analyses. The unconfined compressive strength (UCS) of the composites was investigated after 28 d of hydration. The microstructure, durability, and hydration status of the specimens were evaluated by conducting various tests. Furthermore, the piezoresistive performance of the composite under cyclic loading was investigated using the four-probe and digital image correlation methods.

The outcomes of this study provide insight for the development of new smart structures with applications in civil engineering related to structural layers in transportation infrastructures, especially in critical zones, such as railroad transition zones. This self-sensing composite material will have the capacity to detect material damage, anticipate maintenance needs, and avoid failures, which in some structures may cause fatalities.

2. Materials and methods

2.1. Raw materials

CSS was adopted as the matrix for this study, which was prepared using ordinary Portland cement type I (CEM I 42.5 R) and CEN Standard sand, with siliceous and clean particles. This sand was classified as well-graded sand following the unified soil classification system (USC). The particle size distribution curve and the physical properties of the sand and cement are presented in Fig. 1 and Tables 1 and 2, respectively. The sand grading, measured by sieving, complied with the EN 196–1 and ISO 679: 2009 standard requirements.

In this study, a multi-layer type of GNPs, multi-walled CNTs (MWCNTs), and short CFs were considered as conductive fillers. The characteristics of the GNPs, MWCNTs, and CFs are summarised in Table 3 [40]. Furthermore, the morphology of the hybrid GNPs/CNTs in the dry mix state was investigated via scanning electron microscopy (SEM), as depicted in Fig. 2.

The X-ray diffraction (XRD) patterns of CNTs, GNPs, and CFs are shown in Fig. 3. Pluronic F-127 was used as a noncovalent surfactant to disperse the CNTs and GNPs in an aqueous suspension. PF-127 is a non-ionic triblock copolymer surfactant composed of a central hydrophobic chain of polyoxypropylene and two hydrophilic chains of polyoxyethylene, which are placed on two sides. These molecular structures are similar to that of polycarboxylate, which is typically used as a cementitious composite superplasticizer [43]. For this reason, PF-127 was found to be compatible with cementitious composites and could improve their mechanical behaviour and dry density owing to the improved consistency of the CSS [40].

In addition, tributyl phosphate (TBP, 97%) at half the weight ratio as that of the surfactant was used as an antifoam to prevent pore formation by the surfactant, as previously described [44]. The molecular structures of TBP and PF-127 are shown in Fig. 4 [40]. In this study, concentrated sulfuric acid (H_2SO_4, 98%), hydrogen peroxide (H_2O_2, 30%), sodium nitrate ($NaNO_3$), and potassium permanganate ($KMnO_4$) were utilised for the surface treatment of the CFs, and they were all of the analytical grades.

2.2. Dispersion of CNT/GNP

The unique properties of CNMs greatly depend on their proper dispersion in the composite [20]. Indeed, the existence of strong surface van der Waals forces between CNMs owing to their high specific surface area and aspect ratio is the reason for their high tendency to agglomerate

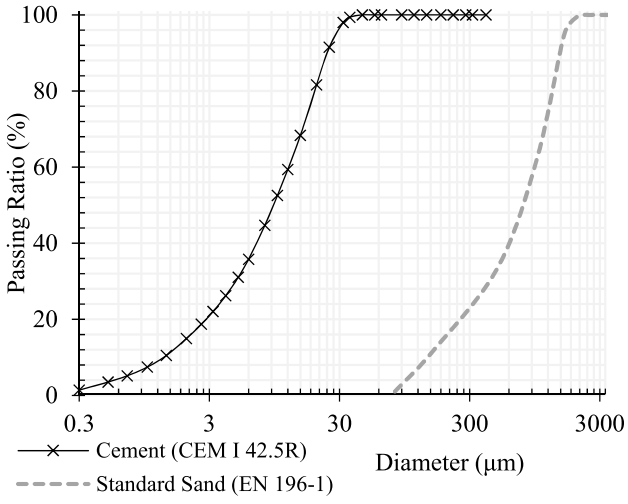

Fig. 1. Particle size distribution curves of cement and sand [8].

Table 1
Physical properties of the sand [8].

Mesh size (mm)	0.08	0.16	0.5	1	1.6	2
Cumulative retained (%)	99 ± 1	87 ± 5	67 ± 5	33 ± 5	7 ± 5	0
Specific gravity G_s	2.67		Cu[a]	7.5	Cc[b]	1.8

[a] Uniformity coefficient.
[b] Curvature coefficient.

[45]. Hence, an effective method is required for the dispersion of CNMs, to transfer the excellent properties of CNT/GNP to the composite [40, 46]. However, the dispersion method should be carefully chosen to prevent adverse effects on the cement hydration process and/or the inherent properties of the nanomaterials [47].

Recently, a compatible and effective method to disperse hybrid CNT/GNP in aqueous suspensions has been developed, which can be used to fabricate multifunctional cementitious composites. In this procedure, TBP was first dissolved in the optimal amount of water required for the fibre-reinforced CSS, by stirring at 800 rpm min^{-1} using a magnetic stirrer for over 12 h. The required optimum water content (ω_{opt}) for each sample of fibre-reinforced CSS was measured by the compaction standard test, for which dry CNT/GNP was dispersed among the dry materials using a mechanical mixer with the gradual addition of water. After completely dissolving the TBP, 10% of PF-127 (by weight of CNMs) was added to the suspension and mixed for 1 h using the magnetic stirrer mixer at the same speed. Based on the literature, the optimal concentration of hybrid CNT/GNP required for the development of a self-sensing cementitious composite is approximately 0.17% (1:1, by weight of the sand), which was estimated by considering the physical behaviour [8,41].

Therefore, the same concentration was used in this study. The hybrid CNT/GNP was added to the suspension and stirred continuously for 1 h, and the suspensions were then placed in a bath sonicator with output power and frequency of 80 W and 45 kHz, respectively, for 3 h. In addition, a digital temperature regulator comprising a circulation system, sensors, and a radiator was used to adjust the temperature during ultrasonication at 40 °C. Under these specific mixing conditions, negligible structural damage was expected for the carbon nanomaterials. Raman spectroscopy (Fig. 5) was performed on the CNMs using laser excitation with a wavelength of 532 nm to ensure the absence of adverse effects on the structural quality of the nanomaterials, such as edge-type defects, decrease in the aspect ratio, and sp^2 domain crystallinity (La), which have a deleterious influence on the mechanical and electrical performances [40,48,49].

2.3. CF surface treatments

The surfaces of the CFs were treated using a chemical method to facilitate the dispersion of fibres and increase the interaction and adhesion between the cementitious matrix and CFs [50–53]. This technique is a novel technique and all details were designed in a way that the chemical reactions and corrosion can be control at a specific level. As this treatment technique is controlled, the measured electrical resistance of the CF didn't show a significant change after treatment.

In this method, CFs were poured into a round-bottomed flask placed in a bath (5 °C) under stirring, and the following were sequentially added (per gram of CFs): 6 g H_2SO_4 (98%) and 0.4 g $NaNO_3$. Subsequently, with continuous stirring, 1.2 g $KMnO_4$ was slowly added to the flask. The solution was held at 5 °C for 1 h until the colour of the solution turned green. The suspension was then heated to 35 °C and stirred for 12 h at this temperature. Then, 20 mL of deionised water was slowly added to the suspension, and while increasing the temperature to 90 °C, 60 mL deionised water and 6 g of H_2O_2 were slowly and sequentially added to the suspension. After this step, the colour of the suspension changed from brown to bright yellow. Then, the suspension was purified by filtration, and the fibres were washed with deionised water

Table 2
Physical properties and chemical composition of the cement [41].

SiO_2 (%)	Al_2O_3 (%)	Fe_2O_3 (%)	MgO (%)	CaO (%)	Na_2O (%)	TiO_2 (%)	K_2O (%)	MnO (%)	P_2O_5 (%)	SO_3 (%)	LOI[a] (%)	Fineness, (m^2 kg^{-1})	Specific gravity (kg dm^{-3})	Initial setting time (min)[b]	Soundness (mm)[b]	Blaine's surface (cm^2 g^{-1})[b]
19.9	4.7	3.38	1.3	63.93	0.17	0.245	0.446	0.079	0.063	2.54	2.97	360	3.15	194	1.1	4220

[a] (Loss on ignition) EN 196–2.
[b] EN 196–3.

Table 3
Characteristics of multi-walled carbon nanotubes (MWCNTs), graphene nanoplatelets (GNPs), and short carbon fibres (CFs) [40,42].

GNP										
Surface area (m^2 g^{-1})	Density (g cm^{-3})	Carbon content (%)	Tensile modulus (GPa)	pH Value (30 °C)	Tensile strength (GPa)	Layers	Dimension		Form	Part Number
120–150	0.6	>99.5	1000	7–7.65	5	<60	Thickness 4–20 nm	Diameter 5–10 μm	Gray Powder	TGN201
MWCNT										
Surface area (m^2 g^{-1})	Density (g cm^{-3})	Colour	Outside Diameter (nm)	Length (μm)	Ash (wt%)		Carbon content (%)	Part Number		
350	0.27	Black	<8	30–10	<1.5		>98	GCM327		
CF										
Diameter (μm)	Length (mm)		Carbon content (%)	Tensile strength (GPa)			Density (g cm^{-3})	Tensile modulus (GPa)		
7	12		≈93	4.9			1.8	230		

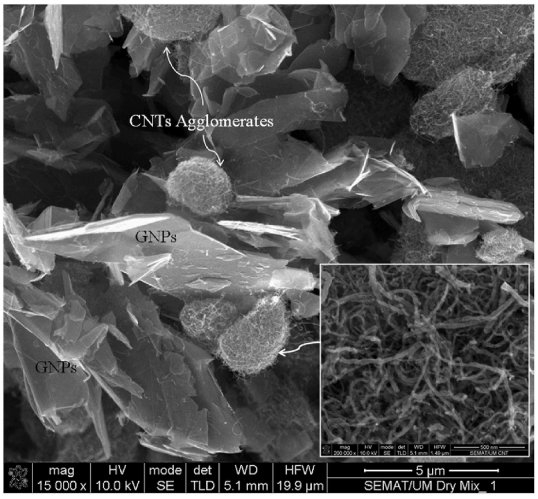

Fig. 2. Morphology of GNPs and CNTs in the dry mix state.

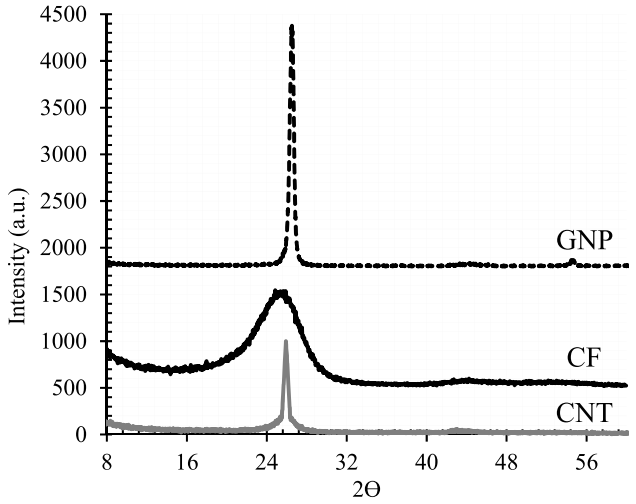

Fig. 3. X-ray diffraction (XRD) patterns of CNTs, GNPs, and CFs.

repeatedly until the washing water contained no SO_4^{2-}. The fibres were then completely dried at 35 °C for 72 h.

2.4. Preparation of CSS

In stabilised sands, the cement content usually varies by approximately 10% owing to the target strength of the sand–cement [54,55]. In this study, 10% of cement (by weight of the dry sand) was used for CSS preparation, and all the specimens were fabricated at the optimum water content (ω_{opt}) determined by performing the standard Proctor test.

First, the treated CFs and sand were added to a steel bowl and blended with a stainless-steel blade at a rotational speed of 140 rpm for 1.5 min. Then, cement was poured into the mixer and blended for 2 min at the same speed. Subsequently, CNM suspensions comprising 0.17% CNT/GNP (by weight of the sand and equal portions, 1:1), prepared with the ω_{opt} (for each CF concentration), were sprayed into the mixture and blended at a speed of 285 rpm for 2.5 min. The concentrations of the CFs

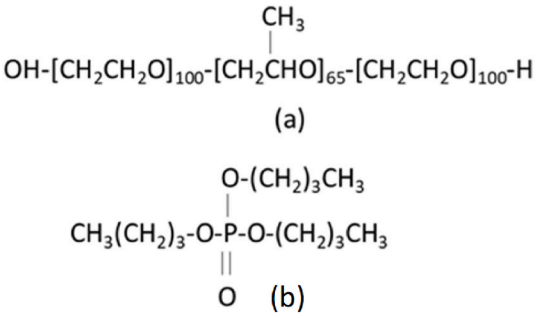

Fig. 4. Chemical structures of (a) Pluronic F-127 and (b) tributyl phosphate 97% [40].

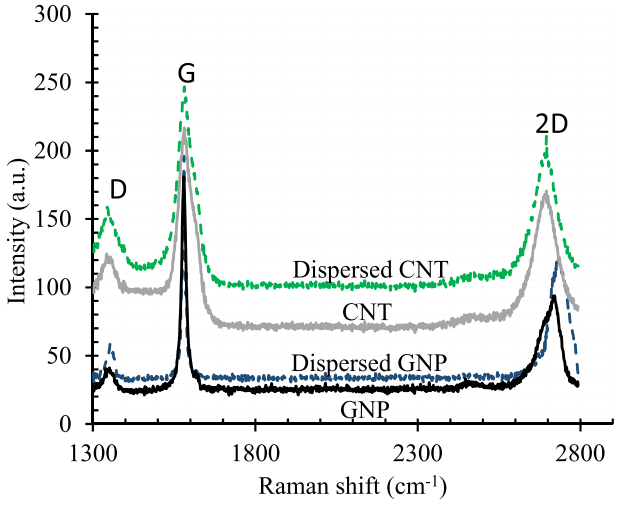

Fig. 5. Raman spectra of CNTs and GNPs after the dispersion process.

used in this study were set at 0.5, 0.75, and 1.0% by weight of the dry sand by considering the physical and piezoresistive behaviour [10,56,57]. The mixture was then placed in a plastic bag to prevent moisture loss. Cylindrical specimens of CSS were fabricated using a standard compaction method as per ASTM D698. Split moulds with dimensions of 101.6 × 116.4 mm were filled with the wet mixture in three equal-height layers. A calculated amount of the well-mixed wet mixture was measured (to an accuracy of 0.01 g), placed into the split moulds, and then compacted carefully by a metal tamper to the desired height (controlled by a calliper to an accuracy of 0.02 mm). After the moulds were filled with the compacted mixture, they were sealed at both ends and extracted after 24 h for hardening. The specimens were then cured underwater for 28 d. Four square pieces of copper mesh with dimensions of 50 mm × 50 mm were embedded in the specimens that were used for piezoresistivity investigations [42]. The moisture in the mixture was measured after compaction to ensure minimal water evaporation. The specimens were named based on their fibre concentration, as listed in Table 4.

2.5. Pullout tests

A single-fibre pullout test was used to investigate the interfacial properties of the CF–cement matrix. Owing to the small size and fragility of the CFs, a special method was used following the literature [59,60]. Special plastic moulds were used to prepare the specimen, which comprised three primary parts: upper units, bottom units, and a frame to fix the position of the CF in the middle of the sample (Fig. 6 (a)).

The thickness of the initial cured specimen was too high, and hence, the single CF broke during the pullout test. Li [61] calculated the theoretical length of CFs to be 5.5 mm for the successful pullout of the fibre without rupture, which shows that the thickness of the specimen, i.e., the length of the CF embedded in the cementitious matrix, should not exceed 5.5 mm.

In fact, to successfully obtain the entire force–displacement curve during pulling out, the real embedded length of the CF should be further limited.

Hence, after 28 d of curing, the specimens were cut to dimensions of 20 mm × 12 mm × 5.0 mm, as shown in Fig. 6 (b). The thickness of the specimen (5.0 mm) was equal to the embedded length of the CF in the cement matrix. The pullout tests were carried out at a rate of 0.02 mm s^{-1} using a universal testing machine. The test results are an average of the values of at least five specimens, and three bonding parameters were calculated as follows [62,63]:

1. Average shear bond strength, τ_{max}, Eq [1].:

$$\tau_{max} = \frac{P_{max}}{\pi d_f l_e}$$

2. Frictional bond strength, τ_{fr}, Eq [2].:

$$\tau_{fr} = \frac{P_{fr}}{\pi d_f l_e}$$

Table 4
Mix proportions of the specimens.

Sample ID[a]	CNT (%)	GNP (%)	CF (%)	Sand (g)	Cement (%)
Plain CSS	–	–	–	1350	10
CG (0.17%)	0.085	0.085	–	1350	10
CGC (0.5%)	0.085	0.085	0.5	1350	10
CGC (0.75%)	0.085	0.085	0.75	1350	10
CGC (1.0%)	0.085	0.085	1	1350	10
CF (0.75%)	–	–	0.75	1350	10

[a] All concentrations are represented with respect to the weight of the dry sand.

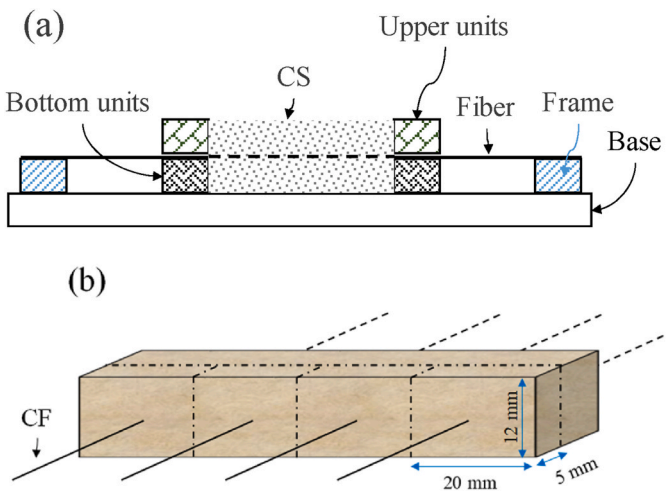

Fig. 6. Specimen fabrication for the pullout test: a) mould cross-section, b) specimen dimensions.

3. Chemical debonding energy, G_d, Eq [2].:

$$G_d = \frac{2(P_{max} - P_{fr})^2}{\pi^2 d_f^3 E_f}$$

where P_{max} is the maximum pullout load, P_{fr} is the frictional pullout load, d_f is the fibre diameter, l_e is the embedded length of the CF, and E_f is the CF elasticity modulus.

2.6. Evaluation of mechanical properties, microstructure, and durability

In this study, UCS tests were used for the mechanical evaluation of CSS following the ASTM/D2166 M standard. The results were calculated as the mean of the values obtained for at least three specimens. Because the modulus of elasticity for cementitious geomaterials is typically expressed by the modulus at 50% of the peak stress [64–66], the tangent $E_{50\%}$ of the specimens was calculated at 50% of the maximum compression stress.

Furthermore, standard compaction tests were carried out following the ASTM D698 standard for evaluating the effects of using different fibre concentrations on the maximum dry density and ω_{opt} of CSS.

In addition, the specimen fracture surfaces were investigated via SEM in the secondary electron mode at an acceleration voltage of 10 kV after coating the specimen with an Au–Pd thin film (30 nm) in a high-resolution sputter coater (Cressington 208HR). Energy-dispersive X-ray spectroscopic (EDX) analysis was performed at 3 kV using an energy-dispersive X-ray spectrometer coupled with SEM. Fourier transform infrared spectroscopy (FTIR) and EDX were performed to analyse the surface chemical composition of the treated fibres. For this purpose, the fibres were purified by washing and precipitating with deionised water and then dried for 10 h at 50 °C in a vacuum-drying container. Thermal analysis of the specimens was conducted to evaluate the cement hydration process using a thermogravimetric analyser (TGA, PerkinElmer) at a maximum temperature of up to 1000 °C and a heating rate of 10 °C min^{-1} in a nitrogen atmosphere (100 mL min^{-1}).

An ultrasonic non-destructive test was conducted for microstructural investigation following the BS EN 12504–4 standard using two probes along the longitudinal axis of the specimens. The weight loss of the fibre-reinforced CSS was measured in terms of composite durability, which was investigated after 12 cycles of wetting and drying according to ASTM D 559–96.

2.7. Methods to investigate piezoresistive behaviour

The four-probe method was used to evaluate fractional changes in the electrical resistivity (FCR) and gauge factors (GF) of CSSs subjected to cyclic axial compression loading. In this method, a 100 Ω reference resistor was connected to the outer probes in a series and was powered by a direct current source (20 V). The details of this measurement are expressed in Ref. [42].

As shown in Fig. 7, three cycles of 5 kN axial compression loading at a rate of 50 N s^{-1} were used to evaluate the piezoresistive behaviour of CSS. Simultaneously, the digital image correlation (DIC) technique was used as a 3D full-field, non-contact optical method to visually monitor the total strain in the specimens during cyclic loading.

3. Results and discussion

3.1. Structural characterization of CFs

FTIR analysis has been used to identify the presence of organic and inorganic compounds in the fibres, owing to the good performance of this method in recognising the decomposition and oxidation of materials [67,68]. The FTIR spectra of the raw and chemically treated CFs are shown in Fig. 8. The results confirm the existence of different functional groups on the surface of the CFs after the chemical treatment.

As can be noticed, the treated CFs possess oxygen groups of -*O*-, -OH, -*C*-SO_3^-, and –COO^-, which is supported by the detection of new peaks at 1356, 1101, 1026 (-*O*-), 3676, 3724 (-OH), 1361, 1263, 981 (-*C*-SO_3^-), and 1728 cm^{-1} (-COOH). The presence of these functional groups on the surface of the fibres can significantly enhance the chemical bonding of the fibres with the cement matrix. In addition, the electrical charges of the functional groups on the surface of the CFs can succour their uniform dispersion in the composite [32,69–71].

The FTIR spectra of both raw and treated CFs showed characteristic peaks at 2154 and 2025 cm^{-1} owing to the stretching vibration of alkaline groups.

Furthermore, the morphology of the CF surfaces was investigated via SEM to qualitatively evaluate the effects of the treatment on the interfacial properties of the fibres. The results are shown in Fig 9 and 10.

As expected, the surface of the CF before modification is comparatively smooth and possesses a slight roughness and few defects. This will certainly militate against proper interface performance, owing to the weak physical friction and interaction between the CFs and the cementitious matrix. However, in Fig. 10, it can be observed that the surface grooves were deepened and more superficial grooves were generated. Furthermore, the treated CFs possessed some irregularities and roughness on the surface of the fibres owing to chemical reactions during the treatment.

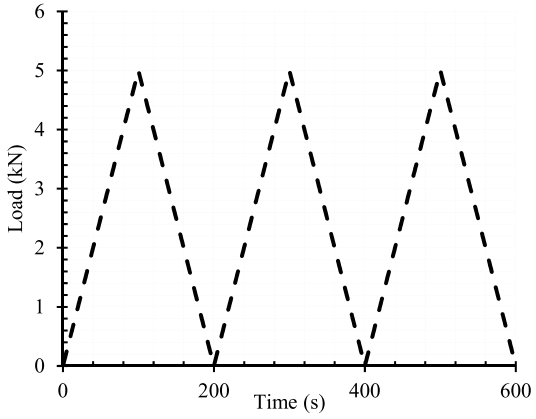

Fig. 7. The cyclic compression loading protocol.

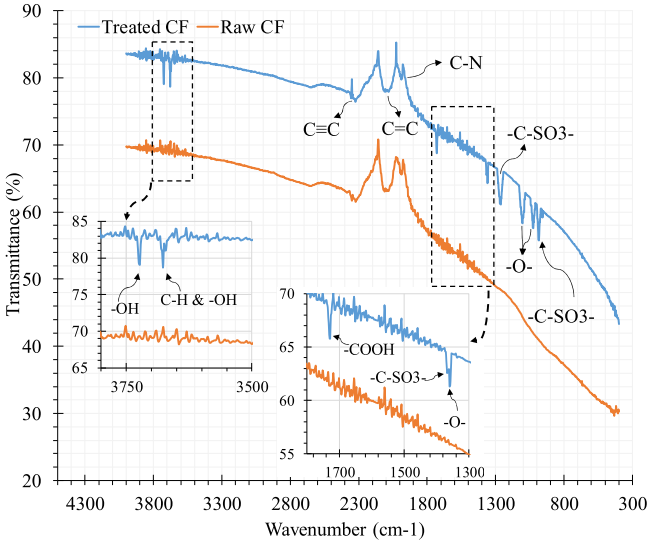

Fig. 8. FTIR spectra of pure and treated CFs.

It is expected that the increase in the surface roughness of CFs will be beneficial for enhancing the fibre surface interaction and strengthening the mechanical join-up between CFs and the cementitious composite [72].

The chemical compositions of the CF surfaces are presented in Table 5. The results show that the CF surface mostly comprises carbon, and the concentration of oxygen is limited to approximately 8%. However, in the chemical composition of the treated CF surface, the amount of oxygen increased to approximately 26%, indicating the oxidation of the surface of the fibres during the treatment process. In addition, the chemical analysis of the CFs confirmed the presence of functional groups including sulphur, nitrogen, and manganese.

The XRD patterns of the raw and treated CFs are shown in Fig. 11. According to the results, the intensity of the CF peaks decreased after the chemical treatment, and the sharp peaks also became broader. The results confirm that the oxygen functional groups penetrated the CF surficial structure.

3.2. Compaction and microstructural investigations

The compaction curves of the plain reinforced CSS and the CSS containing hybrid CNT/GNP and different concentrations of the CF fibre are shown in Fig. 12. The results show that the incorporation of 0.17% (by weight of dry sand) hybrid CNT/GNP into the plain cementitious sand increased the maximum dry density $\gamma_{d(max)}$ of the composite. Furthermore, the addition of 0.5% CF to the specimen containing 0.17% CNT/GNP resulted in a greater increase in $\gamma_{d(max)}$. This trend of increasing dry density continued until the CF concentration was increased up to 0.75%. However, an excessive increase in the CF concentration resulted in a decrease in the maximum dry density. Furthermore, reinforcing plain CSS with 0.75% CF resulted in an increase in $\gamma_{d(max)}$. The $\gamma_{d(max)}$ for this specimen was lower than that of the specimen CGC (0.75%), which contained 0.17% CNT/GNP and 0.75% CF.

With regard to the optimum water content (ω_{opt}), it should be noted that the incorporation of 0.17% hybrid CNT/GNP into plain CSS did not cause a considerable change in the optimum water content. Although the addition of 0.5% CF to this specimen resulted in a decreasing but not significant (8%) trend for ω_{opt}, increasing the CF concentration up to 0.75% reduced ω_{opt} by approximately 18% compared to that of plain CSS. Reinforcing CSS comprising 0.17% CNT/GNP with a high concentration of CF (1.0%) resulted in an abrupt increase in the optimum

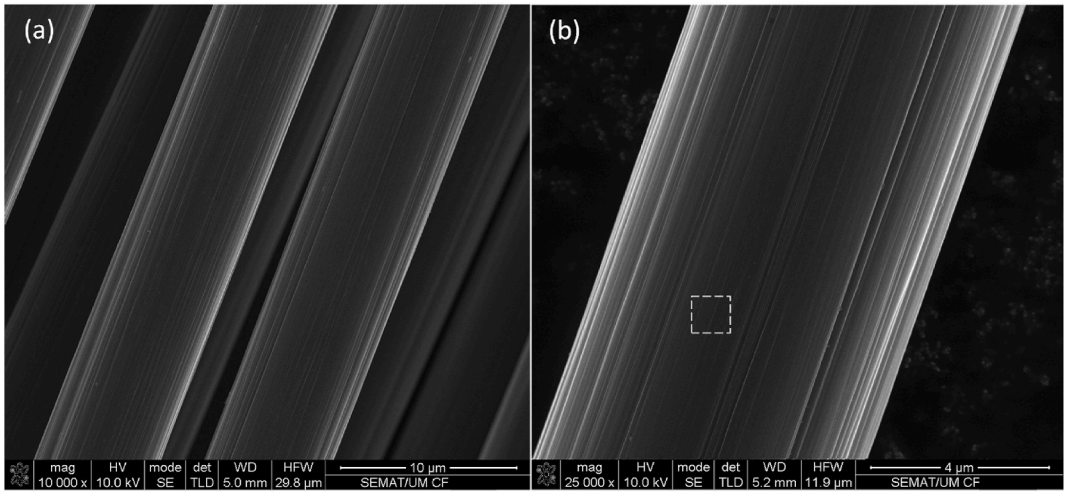

Fig. 9. Surface morphology of the raw CFs (The marked areas in the SEM images are the areas selected for EDX analysis.).

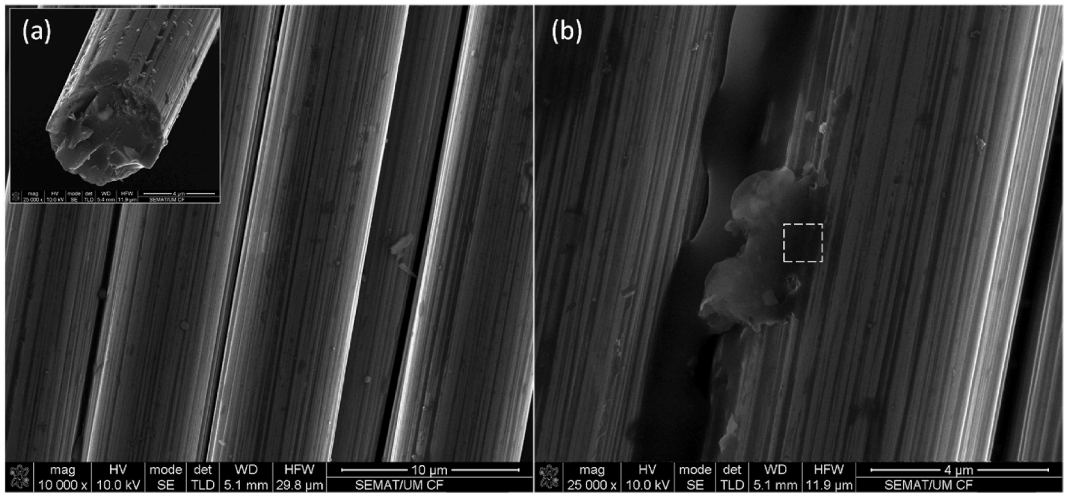

Fig. 10. Surface morphology of the treated CFs (The marked areas in the SEM images are the areas selected for EDX analysis.).

Table 5
Chemical characteristics of raw and treated CF surfaces.

Position	Elements (%)					
	C	O	N	Au	S	Mn
Fig. 9 (Raw CF)	91.73	8.27	–	–	–	–
Fig. 10 (Treated CF)	70.21	26.49	0.61	0.49	1.67	0.53

water content of the composite. Furthermore, the inclusion of 0.75% CF into the stabilised sand in the absence of CNMs reduced ω_{opt} by approximately 15%. Although the filler mechanism of CNTs and GNPs at the nanoscale may seem insignificant because of the nanoparticle size and negligible concentration, these particles can play an important role in the uniform distribution of moisture around the sand grains (Fig. 13). Indeed, the large specific surface area of the dispersed CNTs and GNPs facilitates their high water absorption [41,43,44], which reduces the amount of free water and results in the regular distribution of water.

In addition, the slimy particles of CNTs and GNPs, after water absorption, can act as nano-lubricants around the sand grains to facilitate their slipping and locking together.

In contrast to the CNMs, the filler function of the CFs significantly improved the maximum dry density of the composite. In fact, the high specific surface area, together with the high aspect ratio and flexibility

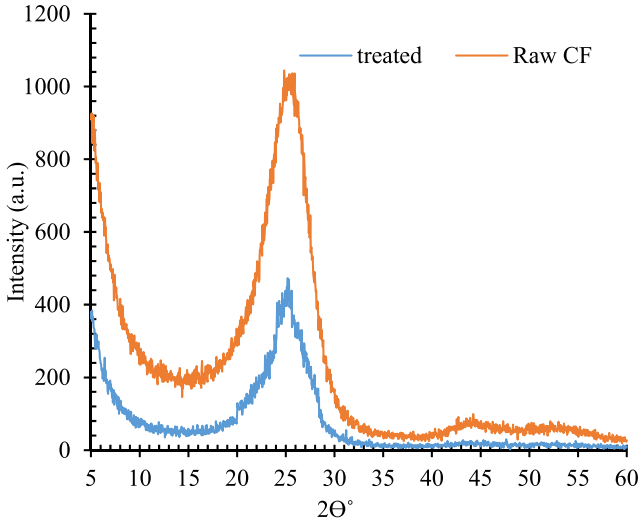

Fig. 11. XRD patterns of raw and treated CF.

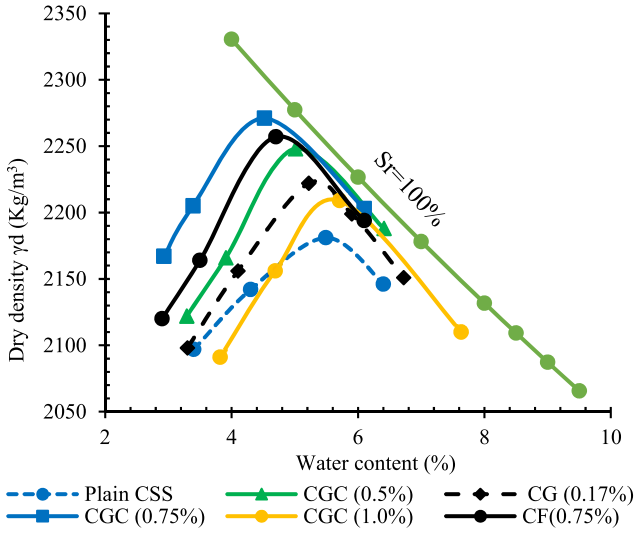

Fig. 12. Compaction curves of CSS specimens with different reinforcements.

of the CF can effectively fill the large variety of gaps and spaces between the sand grains (Fig. 13 (c)).

Although a certain amount of CFs can also act as rollers between the sand, which assists the grains to slide on each other, an excessive increase in CF dosage can cause agglomeration and consequently increase the gaps and space between the grains. Therefore, the maximum dry density decreases, and in contrast, the optimum water content increases.

The degree of saturation for CSS in different reinforcement modes, as shown in Fig. 14, also demonstrates similar trends.

As can be observed, the inclusion of 0.17% hybrid CNT/GNP in the plain CSS increased the degree of saturation to approximately 89%. With the addition of 0.5% CFs to this specimen, the degree of saturation increased again and reached approximately 91%.

Increasing the CF concentration up to 0.75% in the specimen comprising 0.17% CNT/GNP reduced the void ratio and caused an increase in the degree of saturation by approximately 11%. However, because of the excessive increase in the CF concentration to 1.0% in these specimens, the fibres tend to agglomerate, which results in an increase in the void ratio and a decrease in the degree of saturation to approximately 88%.

Reinforcing CSS with only 0.75% CF increased the degree of saturation by approximately 9%. This indicates that the effectivity of 0.75% CF in reducing voids in the composite was lower than that of 0.75% CF together with 0.17% hybrid CNT/GNP.

These interesting outcomes are alternatively demonstrated by plotting $\gamma_d/\gamma_{d(max)}$ vs. "Sr - $(Sr)_{opt}$", as shown in Fig. 15. This unique relationship is in line with the results of recent studies [73] shows that these laboratory outcomes can be applied directly in the field. This supports the practical use of these novel composites.

The ultrasonic wave passing time as a criterion of density changes [74] was measured for the specimens after 1 and 28 d, the results of which are shown in Fig. 16. The results clearly show a similar trend even after 28 d of hydration, proving the above outcomes. The inclusion of 0.17% CNT/GNP in the cementitious composite reduced the porosity,

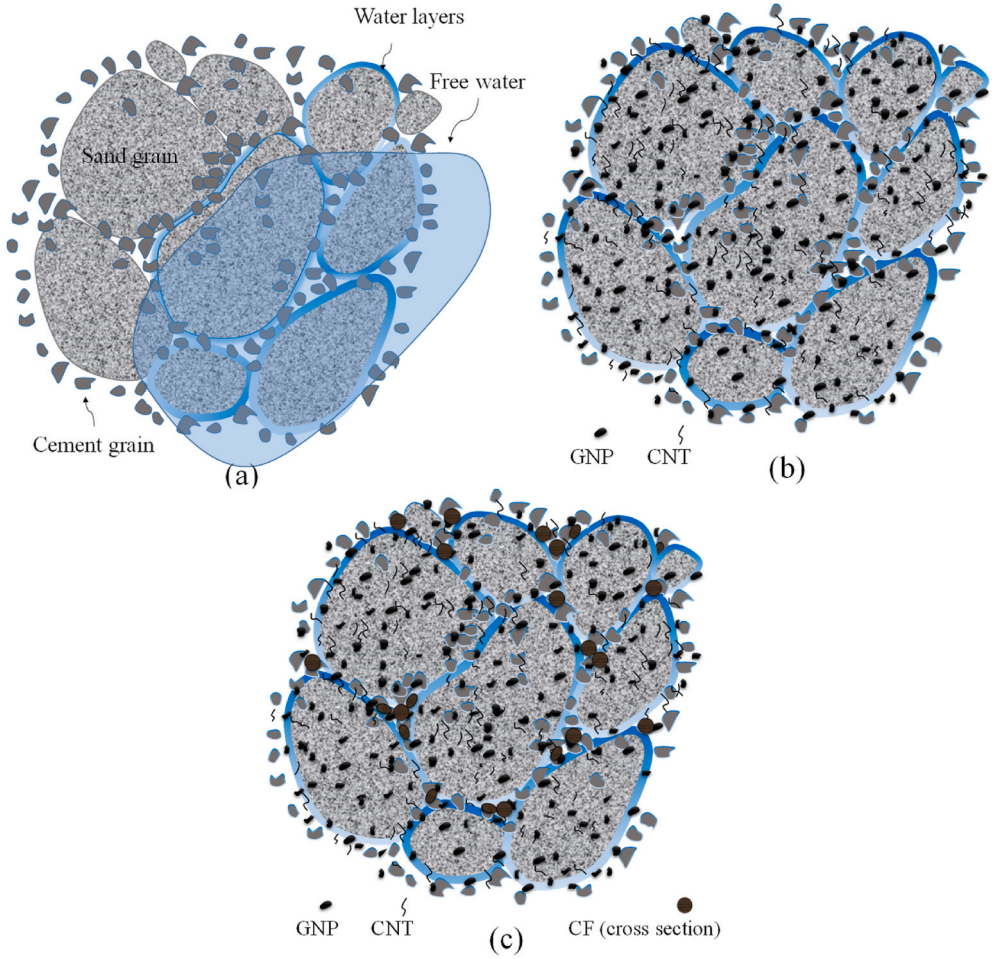

Fig. 13. Schematic of CSS in different reinforcement modes: a) Plain CSS, b) CSS reinforced with hybrid CNT/GNP, c) CSS reinforced with CNT/GNP/CF.

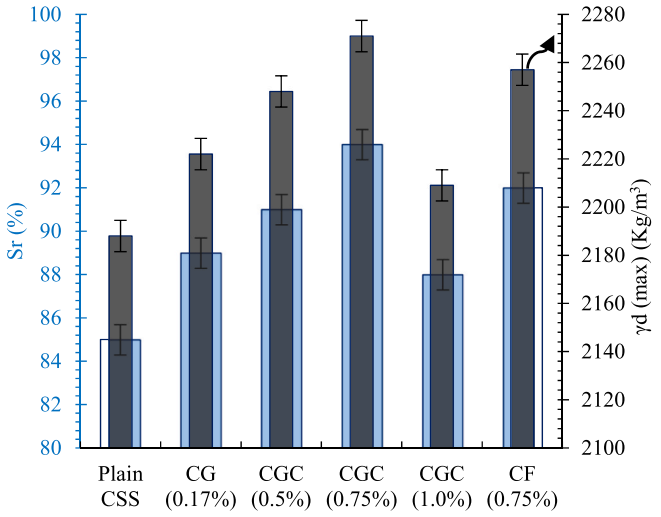

Fig. 14. Degree of saturation (Sr) and maximum dry density (γ_d (max)) of CSS in different reinforcement modes.

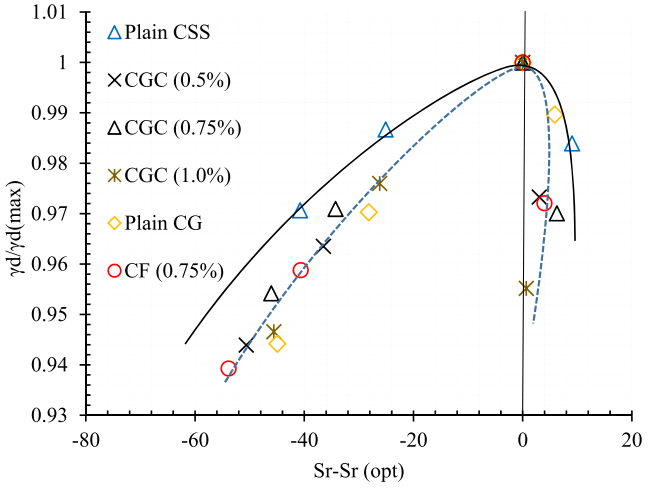

Fig. 15. Relationship between γd/γd (max) and "Sr–Sr (opt).

which decreased the ultrasonic wave passing time for this specimen.

Furthermore, adding 0.5% CF to this specimen and increasing its concentration to 0.75% reduced the wave passing time. However, an excessive increase in the CF concentration resulted in an increase in the ultrasonic wave passing time owing to agglomerate formation. By increasing the age of the specimens and the hydration period, the hydration products of cement grow around the fibres and CNMs and surround them which increases the density and decreases the wave passing time through the specimens. However, the variation in passing time showed that the density enhancement after 28 d was different for each specimen, which could be because of reinforcement effects on the cement hydration process. The reinforcement effect can be attributed to extensive distributing meshwork in the composite, crack bridging, fibre pull-out effect, lowering orientation index of CH crystal in hydration products [75,76], which are discussed further in the following sections.

Notably, the CNMs buried among the hydration products act as nanoscale reinforcements. In fact, a certain amount of CNMs can reduce the nano cracks by bridging and/or deviation mechanisms (Fig. 17) and prevent their propagation which can consequently enhance the mechanical properties of the composite.

Because of the tubular and 2D geometrical shapes of CNTs, they

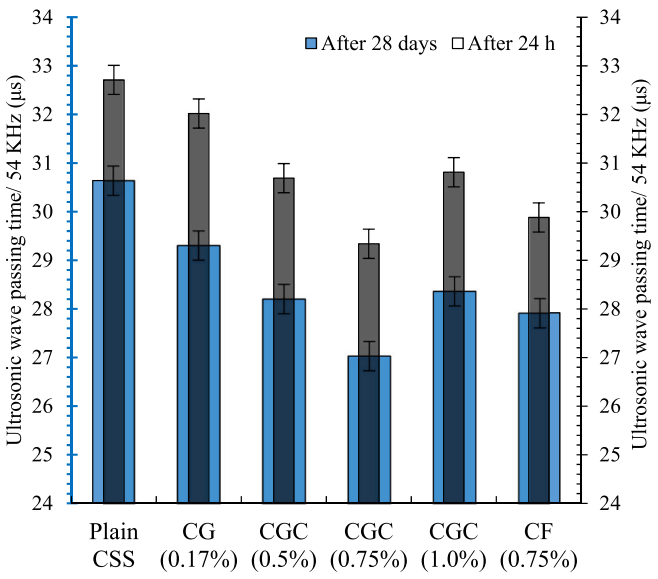

Fig. 16. Ultrasonic wave passing times for different reinforced CSS after 1 and 28 d.

could be most effective at crack bridging, whereas the GNPs with 1D and plate-like geometrical shapes could also deviate the path of the cracks. As the stress on the specimen increases, nanoscale cracks also grow and develop. Meanwhile, owing to an increase in the crack mouth opening displacement, at their joining, microcracks are generated. However, the micro-CFs were activated to prevent the propagation and growth of microcracks (Fig. 18). In such a situation, at least two mechanisms can occur.

In the case of weak interfacial properties of fibre and cement composite, fibres creep in the early stages and are finally pulled out or extruded from the cement matrix with a further increase in applied stress.

By improving the interfacial properties and adhesion of the fibre in the cement matrix, the applied stresses are mobilised as shear stresses on the surface of the fibres. Furthermore, as long as these stresses do not exceed the friction bond strength of the fibres and matrix and/or their tensile strength, the fibres can prevent crack propagation. Indeed, this behaviour, which causes a significant enhancement in the ductility and mechanical properties of the composite, is one of the advantages of using multiscale reinforcements.

3.3. *Interfacial performances of CFs*

Because the bond characteristics of the fibre and matrix play a crucial role in the mechanical performance of fibre-reinforced composites [60,63,77], it is necessary to investigate the interfacial properties of the fibre matrix in terms of physical and chemical bonding. Thus, the raw and treated CF-reinforced cementitious composites were observed via SEM after different hydration periods, as shown in Fig 19 and 20. It can be clearly seen that there is no regulation and a significant amount of cement hydration products are present on the surface of the raw fibres. Furthermore, it appears that these products do not have a strong bond or adhesion with the fibre and are simply detached from the surface (Fig. 19 (b)). In contrast, the surface of the modified CF is completely covered by cement hydration products.

The surface of the treated CF is composed of many oxygen-containing functional groups, such as -*O*-, –OH, -*C*-SO_3^-, and –COOH, owing to the chemical treatment. In the early stages of the cement hydration process, the active functional groups reacted preferentially with cement compounds such as tricalcium silicate, dicalcium silicate, and tricalcium

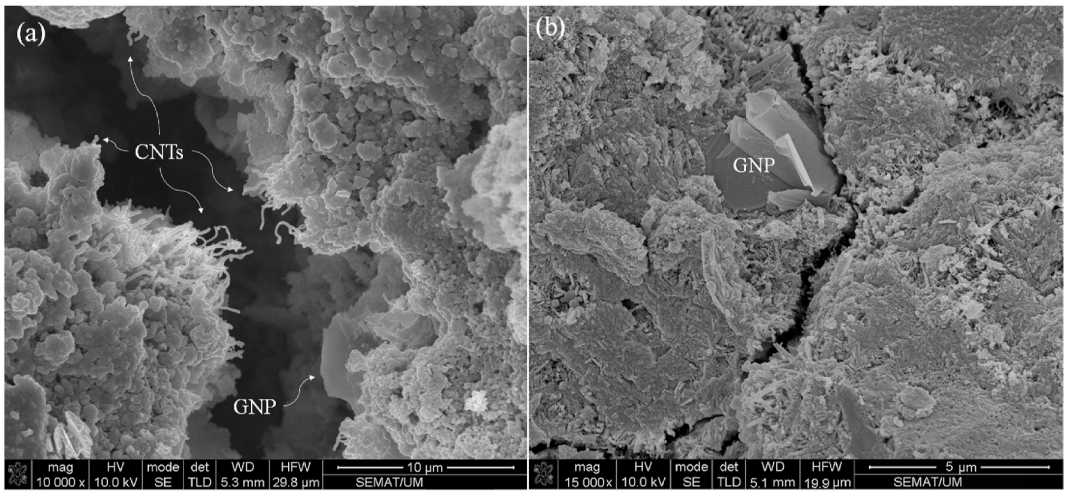

Fig. 17. Mechanism of crack bridging and deviation by CNTs and GNPs.

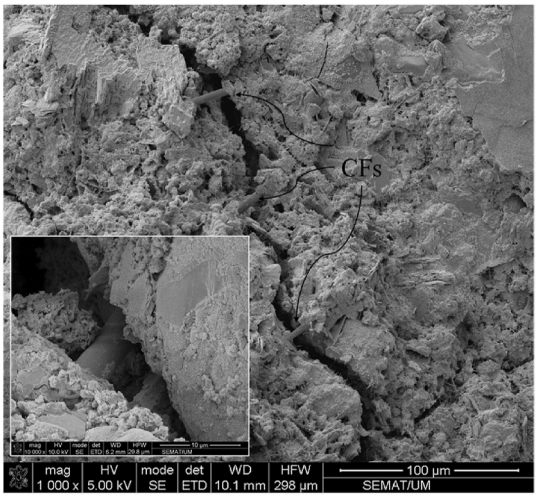

Fig. 18. Mechanism of microcracks bridging by CFs.

aluminate, generating the growth points of the hydration products (Fig. 20 (a)). As the hydration process progresses, the hydration reaction continues to occur at the growth points on the surface of the CFs. The growth points and patterns of the cement hydration products can be regulated and controlled by the CFs, which is called the template effect. The thickness and density of the layer created by hydration crystals on the surface of the CFs may apparently increase with the age of the specimen and the hydration period (Fig. 20 (b)).

To analyse the hydration crystals on the surface of the CFs, EDX analysis was conducted, and the results are listed in Table 6.

The elemental composition of the hydration crystals on the surface of the modified CFs is similar to that of CH and *C*–S–H [24,41]. However, the low percentages of oxygen, calcium, and silica on the surface of raw CF can indicate the absence of cement hydration products on the surface of the raw fibres.

To further investigate the interfacial properties of the CFs, XRD and FTIR analyses were conducted on raw and modified CFs extracted from cementitious composites, whose spectra are shown in Fig. 21.

As can be observed in Fig. 21 (a), the XRD pattern of the treated CFs shows several peaks related to the cement hydration products, including CH and *C*–S–H. However, in the XRD pattern of the raw CFs, almost no trace of cement hydration products is observed.

In Fig. 21 (b), a strong absorption peak is present at 1430 cm^{-1} in the FTIR spectrum of the surficial products of the treated CFs, which is characteristic of *C*–S–H [60,78]. In addition, the FTIR spectrum of the treated CFs showed characteristic peaks at 3645 and 970 cm^{-1}, which are related to the stretching of *O*–H in $Ca(OH)_2$ and *Si*–O in SiO_4,

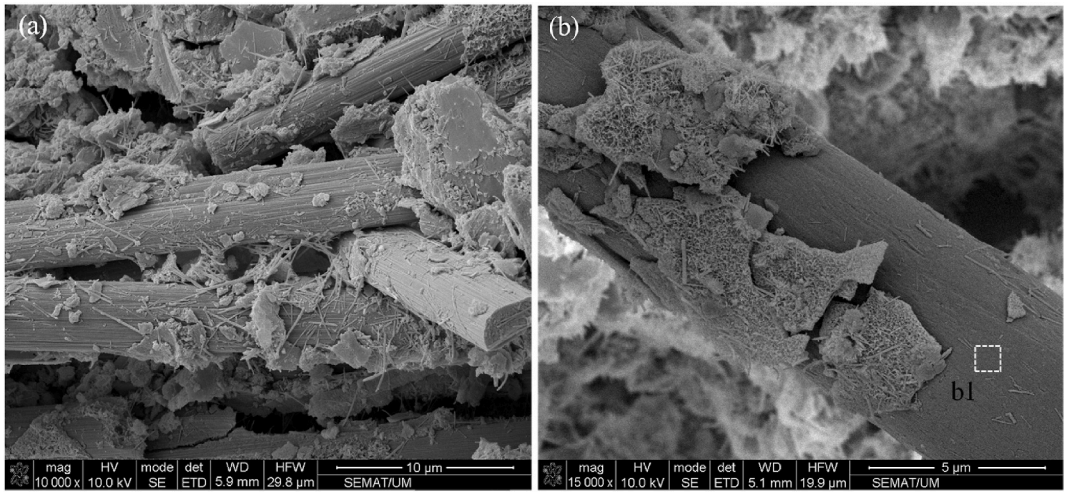

Fig. 19. Raw CFs among the cementitious composite (The marked areas in the SEM images are the areas selected for EDX analysis.).

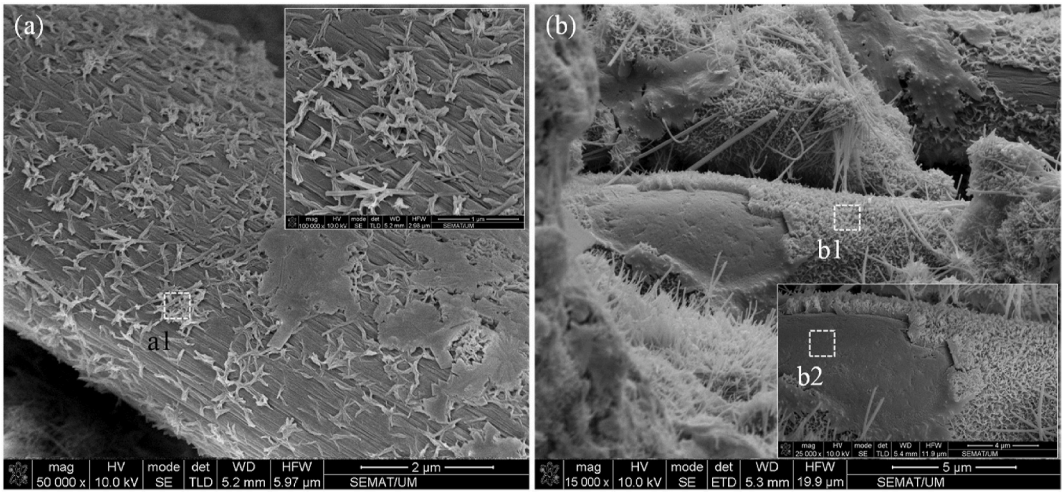

Fig. 20. Treated CFs among the cementitious composite, a) after 1 d and b) after 28 d (The marked areas in the SEM images are the areas selected for EDX analysis.)

Table 6
Results of elemental analysis of the CF surface extracted from the cementitious composite.

Position	Elements (%)										
	C	O	Fe	Ca	Al	Si	S	Mg	Au	Mn	K
Fig. 19 (b), b1	53.11	12.72	1.44	11.31	5.62	9.91	1.34	1.17	1.12	1.67	1.52
Fig. 20 (a), a1	31.8	21.6	1.12	21.76	1.14	19.16	–	0.91	0.85	0.58	1.22
Fig. 20(b), b1	21.34	26.81	1.36	23.93	1.29	21.95	1.11	1.47	0.61	–	0.69
Fig. 20 (b), b2	44.26	16.15	1.61	16.37	3.42	13.15	1.82	1.26	0.86	0.42	0.77

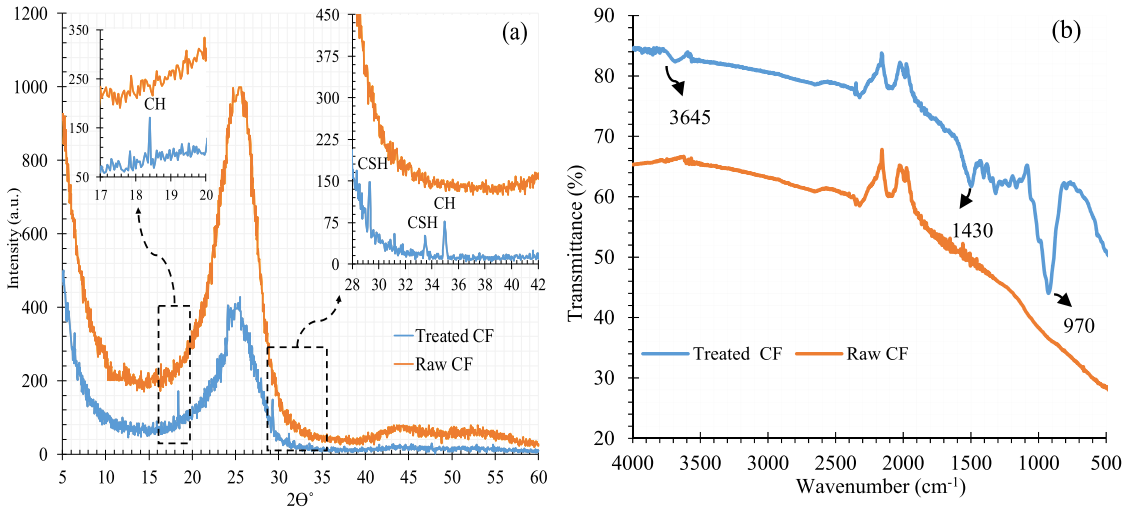

Fig. 21. Chemical characterization of fibres extracted from the cementitious composites: a) XRD patterns, b) FTIR spectra.

respectively [79].

These results indicate that owing to the presence of different surficial functional groups, the modified CFs can react with the compounds of cement hydration to form *C*–S–H and CH, resulting in an improvement in the interfacial adhesion of the CFs with the cementitious composite.

To analyse the mechanical properties of CFs, interfacial properties such as bond strength (τ_{max}), frictional bond strength (τ_{fr}), and chemical debonding energy (G_d) were estimated via pullout tests. The single-fibre pullout test provided a direct display of the interfacial performance of the CFs in the cementitious composite [60,78]. Typical results of successful pullout tests are shown in Fig. 22.

The pullout curves (Fig. 22(a)) reveal the specifications of the pullout and bond properties of the CFs within the composite.

The pullout curves of the CF can be divided into three phases. The first and linear phase is mainly related to the elastic stretching of CFs under a pull force before the full debonding of the interface.

The pull force decreases abruptly to P_{max} after reaching the peak value (P_{fr}) and forms the second phase of the curve. The sudden drops in the pull force are indicative of the chemical bond of CF and the cementitious matrix (G_d) [60,63,78]. The pullout curve steps into the slippage phase by complete debonding, and the CF begins getting pulled out from the composite. Subsequently, the force of interfacial friction controls the pull force, and the movement of the CF from the composite causes a large displacement in the curve.

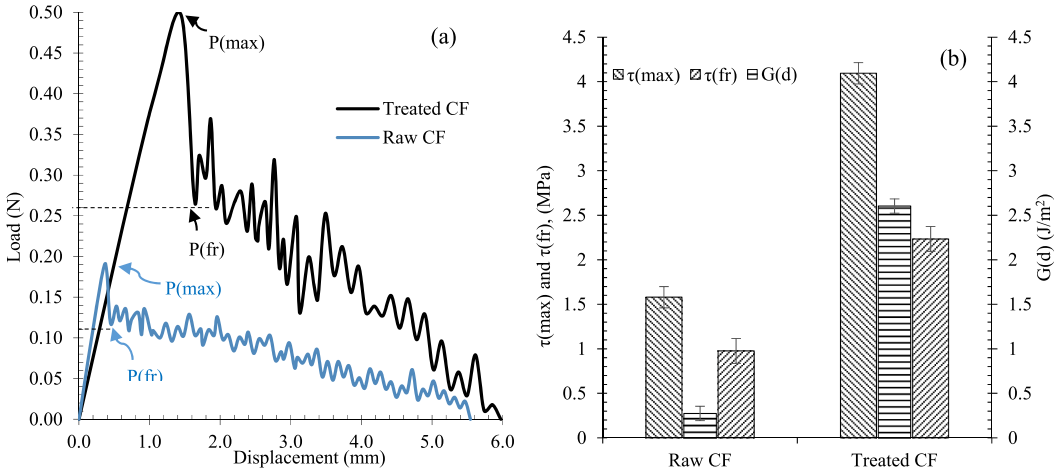

Fig. 22. Single-fibre pullout test results of raw and treated CFs: a) Pullout curves, b) Interfacial properties.

With the CF being pulled out from the specimen, the frictional surface is reduced which results in a linear decrease in the pull load (frictional force) upon displacement. This indicates that no slip-hardening or slip-softening effect occurs for CF in the cementitious composite [60]. However, it has been observed for other fibres in the cement matrix [80].

Finally, the frictional force reached zero when the CF was pulled out from the specimen, and the total displacement was approximately equal to the CF embedment length. According to studies on fibre pullout from cement and polymer matrices, the interfacial shear stress is not constant [81,82]. Indeed, the maximum interfacial shear stress occurs at the beginning of embedment, and before reaching the bond strength, the debonding will first fall at this point. Accordingly, the bond strength obtained using Eq [1]. cannot be the actual bond strength of the fibre–matrix interface. However, this bond strength is important as it is the reflection of the extensive capacity of the embedded CFs to bridge the cracks [80].

Fig. 22 (b) shows the interfacial properties including τ_{max}, τ_{fr}, and G_d for the raw and treated CFs in the cementitious composite.

The frictional bond strength and chemical debonding energy contribute to the bond strength of the fibres. The chemical debonding energy (G_d) and frictional bond strength (τ_{fr}) of the raw CF are approximately 0.27 J m^{-2} and 0.97 MPa, respectively, and the bond strength (τ_{max}) for this fibre was approximately 1.57 MPa. This result shows that the frictional bond strength plays a crucial role in the bond strength of raw CFs in the cementitious matrix.

In the case of treated CF, the chemical debonding energy, frictional bond strength, and bond strength were all greatly increased and were 2.6 J m^{-2}, 2.23 MPa, and 4.09 MPa respectively, which are approximately 10, 2, and 3 times higher, respectively, than those of raw CF. Hence, the enhancement in the bond strength of the treated CF is mainly related to the significant improvement in the chemical adhesion. However, the frictional bond strength also increased considerably.

3.4. Investigation of cement hydration process

The main components of the cement in the anhydrous state are tricalcium silicate (Ca_3SiO_5, abbreviated as C_3S), tricalcium aluminate ($Ca_3Al_2O_6$, C_3A), tetracalcium aluminoferrite ($Ca_4Al_nFe_{2-n}O_7$, C_4AF), and dicalcium silicate (Ca_2SiO_4, C_2S), along with small amounts of gypsum ($CaSO_4{\cdot}2H_2O$) and clinker sulphate (Na^2–SO_4, Ka_2SO_4) [41]. These compounds react with water during the cement hydration process to produce monosulphonate (AFm), ettringite (AFt), calcium silicate hydrate (*C*–S–H) gel, and calcium hydroxide (CH) [24,83]. During these processes, the formation of hydration products with various geometries and crystal shapes plays a key role in determining the final properties of the cementitious composite.

To investigate the possible effects of CFs and CNMs on the cement hydration process, TGA was performed, and the results are shown in Fig. 23 (a). In addition, the results of differential scanning calorimetry (DSC) are shown in Fig. 23 (b) to better understand the temperature range associated with each weight decay. A range of weight losses was observed in the TGA curves between 105 and 1000 °C for the cementitious composite powder, as found in previous studies [84,85].

In the TGA curves, the first drop was observed up to 105 °C, which could be related to the free water and moisture elimination of the sample.

The second decay occurred between 105 and 400 °C which is attributed to the dehydration of chemically bound water existing in hydrated materials such as ettringite, *C*-A-*S*-H, carbo-aluminates, and *C*–S–H. The next large weight loss was detected between 400 and 550 °C, which could be the result of CH dehydroxylation. The fourth and final decay in the TGA curves was because of calcium carbonate and clinker carbonation, which was observed between 550 and 800 °C [41].

As shown in Fig. 23, the incorporation of 0.17% hybrid CNT/GNP increased the amount of CH and *C*–S–H gel formed. The positive effects of CNMs on the cement hydration process have been reported previously [86,87]. CNMs can increase and accelerate the formation of numerous cement hydration products owing to their behaviour as nucleation agents or nano-core effects [41]. Indeed, the nano-core effect is the result of the hybrid nano effect and core effect of nano-fillers incorporated into the cementitious matrix. The cement hydration products will deposit on the CNMs owing to their high surface energy and ultra-high specific surface area. In addition, some of the CNMs can react with the hydration products. Besides numerous nano-fillers are dispersed in the composite, due to the small size of the CNMs. As a result, the CNMs serve as nano-cores [88,89].

The results indicate that the addition of CF and increasing its concentration in the specimen containing 0.17% CNMs consistently decreased the rate of hydration compared to that in the specimens consisting of only CNMs. This is probably because of the reduction in the specific surface area of CNM fillers by the addition of microscale CFs, which reduces their nucleating effects. However, the amount of hydration products in these specimens is not less than that in plain CSS, even in the specimen with a high CF concentration. Moreover, even the inclusion of only 0.75% CF in the CSS caused slight changes in the amount and/or rate of formation of hydration products.

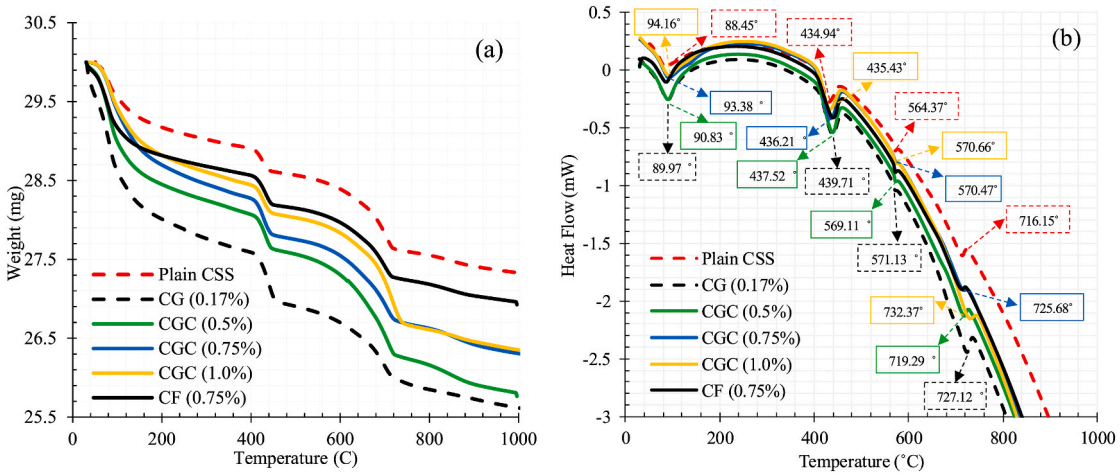

Fig. 23. Thermal analysis result of cement hydration products: a) TGA curves, b) DSC curves.

3.5. Mechanical characterization

To investigate the mechanical properties of plain and reinforced CSS in different cases, the UCS test was performed, and their stress/strain curves together with $E_{50\%}$ are shown in Fig. 24.

The results indicate that the incorporation of 0.17% hybrid CNT/GNP increased the UCS and $E_{50\%}$ of the plain CSS by approximately 24% and 30%, respectively. Furthermore, reinforcing the specimen containing 0.17% CNT/GNP with 0.5% and 0.75% CFs resulted in an increase in the UCS by approximately 52 and 96%, respectively; however, they decreased the $E_{50\%}$ by approximately 11 and 16%, respectively. Notably, an excessive increase in the CF concentration to 1% resulted in a decrease in the UCS. In addition, the inclusion of 1% CF into the specimen CG (0.17%) decreased the $E_{50\%}$ by approximately 32%.

Regarding specimen CF (0.75%), which comprised only 0.75% CF, the UCS increased by approximately 63%, whereas the $E_{50\%}$ decreased by approximately 14% compared to that of plain CSS.

The above outcomes, which are in line with those discussed in the previous sections, indicate the preferential and positive effects of multiscale reinforcement in terms of increasing the compression strength and ductility of the CSS.

3.6. Investigations on durability and permeability

For geomaterials, the hydraulic conductivity and durability of the composite against destructive environmental factors are important parameters that have a significant impact on the stability and long-term performance of the composite [90,91] and should be evaluated in any reinforcement plan. In this study, the durability of plain and reinforced CSS against wet and drying cycles was evaluated as it is one of the most conventional environmental cycles. In this approach, the weight losses of duplicate specimens, in addition to the permeability coefficient, were measured for different reinforced specimens, as shown in Fig. 25.

Plain CSS demonstrated a weight loss of 3.11% after 12 wet and dry cycles; however, the inclusion of 0.17% hybrid CNT/GNP in plain CSS can decrease the weight loss of the specimens to approximately 2.48%, which indicates a 20% improvement in weight loss. However, reinforcing this specimen with 0.5% CFs decreased the weight loss by approximately 38%. In addition, increasing the CF concentration to 0.75% in this specimen caused a further decrease in the amount of weight loss. The weight loss of the specimen CGC (0.75%) was only 1.21%, which indicates a 61% improvement over that of plain CSS. However, an excessive increase in CF concentration (1.0%) resulted in a downward trend, to the extent that the weight loss of the specimen CGC (1.0%) compared to that of plain CSS was not significantly different. Furthermore, reinforcing plain CSS with only 0.75% CFs resulted in a

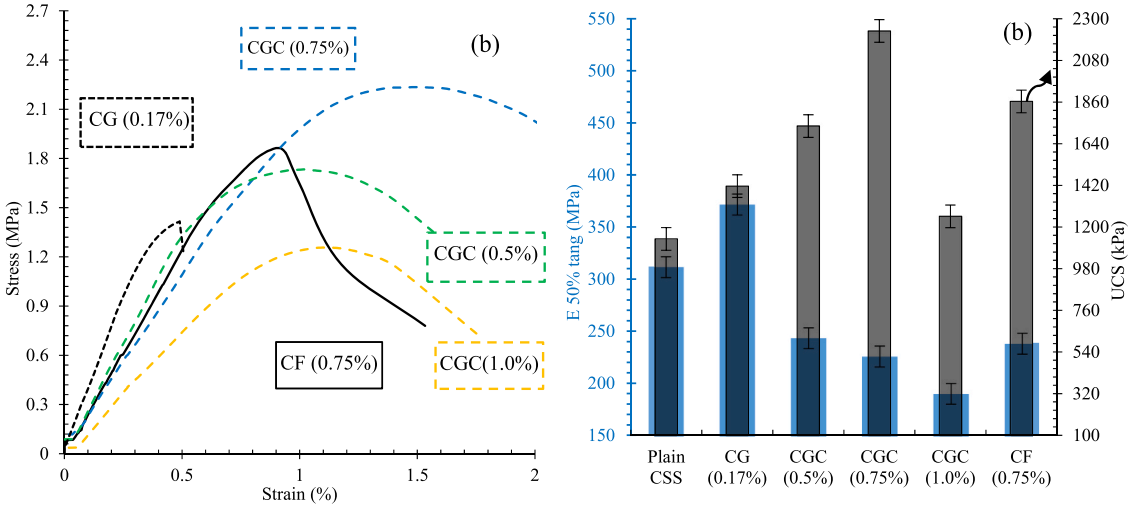

Fig. 24. Mechanical properties of different reinforced CSS specimens: a) stress/strain curves, b) UCS and $E_{50\%tang}$.

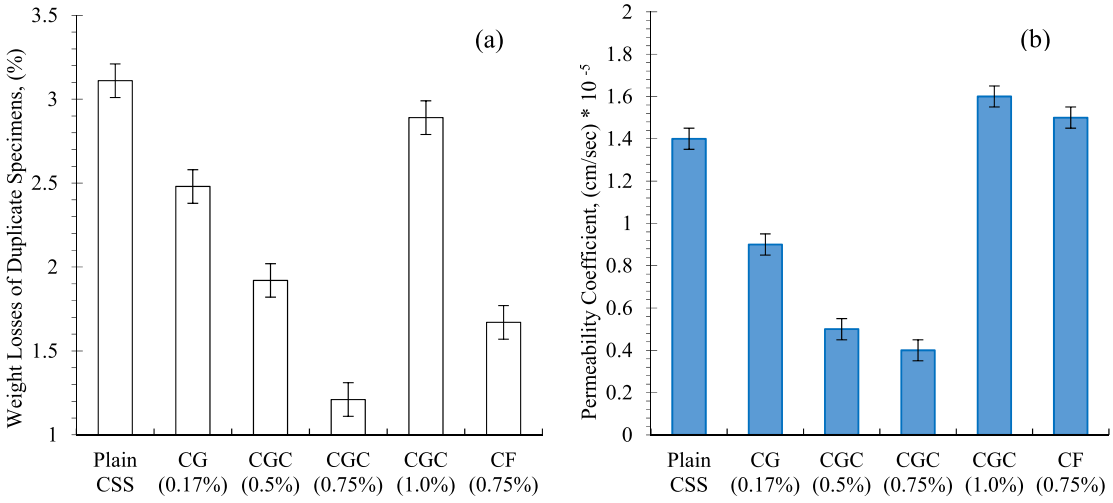

Fig. 25. Results of the investigation of durability and permeability: a) weight losses of duplicate specimens, b) permeability coefficient.

significant improvement in the weight loss by approximately 46%.

Regarding the hydraulic conductivity of the composites, from the permeability coefficient results, the incorporation of 0.17% CNT/GNP into plain CSS decreased the permeability coefficient of the specimen by around 35%. Additionally, the specimen CGC (0.5%), which comprised 0.17% CNMs and 0.5% CF, demonstrated a 64% decrease in the permeability coefficient compared with that of plain CSS. Furthermore, increasing the CF concentration to 0.75% in this specimen decreased the permeability coefficient by approximately 71%. Increasing the CF beyond that resulted in an increase in the permeability coefficient by approximately 14% compared with that of plain CSS. Furthermore, the results showed that the inclusion of only 0.75% CFs in plain CSS did not lead to a significant change in the permeability.

These results, which are heavily dependent on the physical and microstructural properties of the composite, also proved the high potential and efficiency of multiscale reinforcement in cementitious composites.

3.7. Investigations of electrical behaviour

3.7.1. Electrical conductivity

The electrical resistivity of reinforced CSS, with different types of reinforcement, after 72 h of oven drying is shown in Fig. 26. As can be seen, although the incorporation of 0.17% hybrid CNT/GNP resulted in satisfactory electrical conductivity ($\rho \approx 32\ \Omega$ m) in the cementitious geocomposite, the addition of 0.5% CF resulted in a further decrease in the electrical resistivity of this specimen. Indeed, the electrical resistivity of specimen CGC (0.5%), which comprised 0.17% CNMs and 0.5% CFs, demonstrated a decrease of approximately 40% compared with that of the specimen CG (0.17%), which contained only 0.17% CNMs.

Increasing the CF concentration to 0.75% and 1.0% in this specimen persistently decreased the electrical resistivity by approximately 64% and 72%, respectively, compared with those of the specimen CG (0.17%). The electrical resistivity of specimen CGC (1.0%) was slightly lower than that of specimen CGC (0.75%), indicating that the percolation threshold concentration can be in the range of 0.75–1.0% in the case of CNT/GNP/CF reinforcement. Notably, the electrical resistivity of specimen CF (0.75%), which comprised only 0.75% CF, was obtained 2 and 5.5 times more than that of specimens CG (0.17%) and CGC (0.75%), respectively. This indicates the high potential of hybrid CNT/GNP in terms of electrical conductivity enhancement relative to CFs and the higher potential of their triple combination (CNT/GNP/CF) compared with their individual applications in cementitious

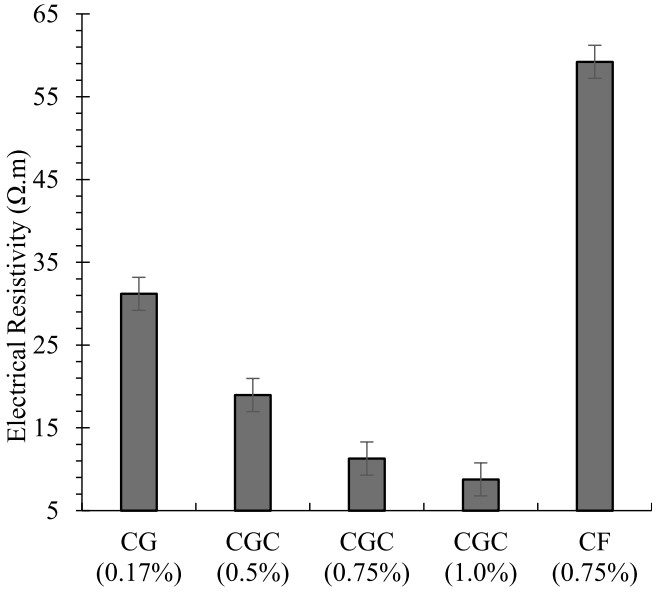

Fig. 26. Electrical resistivity of reinforced CSS in different cases after 72 h of oven-drying.

geocomposites. As illustrated in Fig. 27, the inclusion of CF in the specimen comprising hybrid CNT/GNP and increasing its concentration, in addition to percolation augmentation and increasing conductive paths, reduces the electrical resistance by bridging and connecting the conductive regions formed by the CNMs and ions.

In comparison to the results of other studies about cementitious composite (Table 7), It is clear that the triple combination of CNT/GNP/CF offers higher efficiency in terms of reducing the electrical resistivity of the composite.

3.7.2. Piezoresistive behaviour under cyclic compression test

The variations in the axial strain and fractional changes in the electrical resistivity under cyclic compression loading for reinforced CSS in different cases are shown in Fig. 28. Owing to a decrease in the electrical resistance during compression loading relative to the primary electrical resistance of the specimen, negative values were measured for FCR [42].

Indeed, the conductive fillers and paths during compression loading

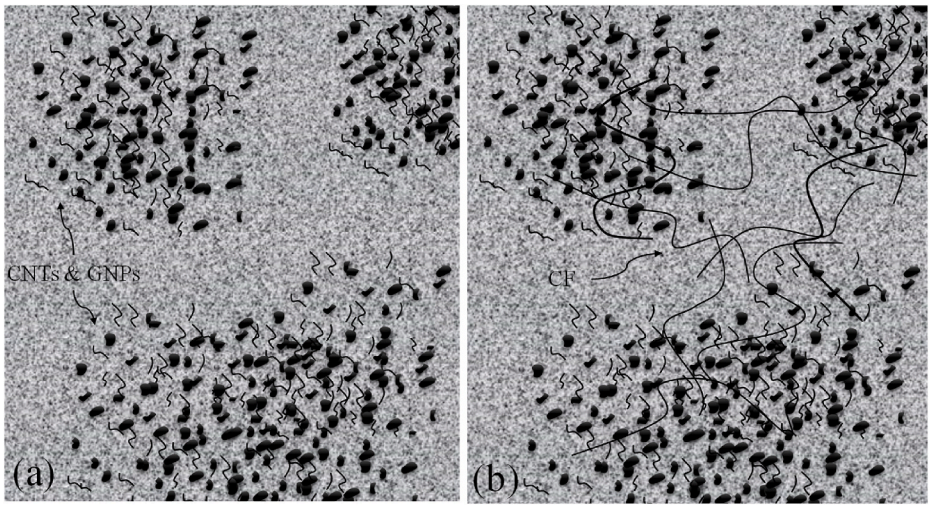

Fig. 27. Schematic of conductive paths: a) CNT/GNP reinforced CSS, b) CNT/GNP/CF reinforced CSS.

Table 7
Comparison among different studies regarding cementitious composites with carbon-based fillers.

Matrix	Nanoparticles type	Filler concentration (%)	Electrical resistivity (Ω. m)	References
Mortar	GNP	5 (wt)	21.02	[92]
Paste	CNF	2 (wt)	11	[93]
Mortar	GNP	5 (wt)	78.2	[92]
Mortar	GNP	5 (wt)	27.96	[92]
Mortar	CNT	0.7 (wt)	24	[94]
Mortar	Graphene	1 (wt)	4000	[95]
Mortar	Carbon Black	10 (wt)	4.53	[96]
Paste	GNP	4.8 (wt)	20	[97]
Mortar	CF	2 (wt)	2.4	[98]
Mortar	CNT/NCB	1.5 (vol)	7.83	[21]
Mortar	CNT/GNP	1 (wt)	15.3	[8]
Mortar	GNP/CNT/CF	0.085/0.085/1 (wt)	8.7	Present Study

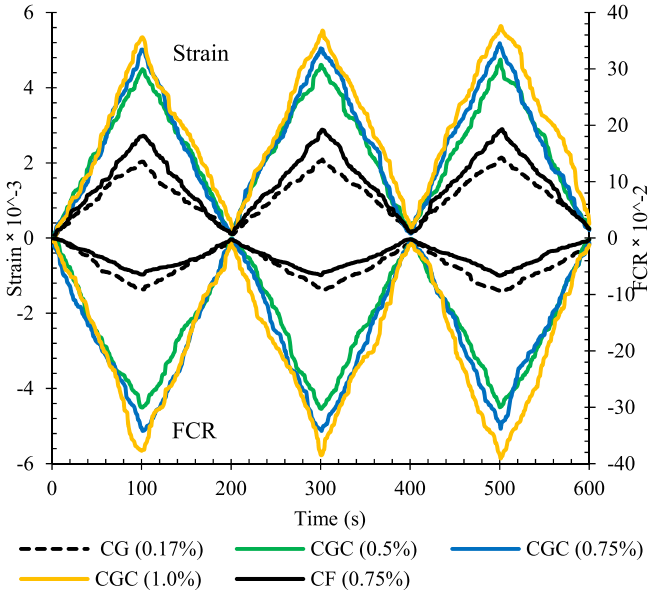

Fig. 28. Variation of the axial strain together with fractional changes in the electrical resistivity (FCR) for different reinforced CSS specimens.

get closer together, and more conductive pathways are formed, which results in decreased electrical resistivity and consequently improves the electrical conductivity of the specimen. As can be seen, different FCRs were achieved in the reinforced composites according to the type and concentration of the conductive fillers. However, a similar compressive cyclic load was applied to the specimens. This indicates that the piezoresistive behaviour and sensing capacity of the CSS are affected by the type and concentration of the conductive fillers. However, the FCR behaviours of all the composites were similar to the cyclic compressive loads, regardless of the volume fraction. The FCR increased upon loading and decreased upon unloading. This is because, as Wen and Chung stated [99], the external load affects the shape and distance of conductive fillers and paths. This indicates that the electrical resistivity decreased upon loading, whereas it increased upon unloading. Thus, the specimen comprising hybrid CNT/GNP exhibited a lower amount of FCR compared to the specimen reinforced with CNT/GNP/CF. However, the amount of strain in this specimen was also lower than that in those reinforced by CNT/GNP/CF. In addition, increasing the CF concentration in specimens containing CNT/GNP/CF resulted in an increase in the amount of FCR, such that the maximum FCR and strain were obtained for specimen CGC (0.1), which comprised 0.17% CNMs and 1.0% of CFs. Regarding specimen CF (0.75%), which contained only 0.75% of CFs, although this specimen exhibited a higher amount of strain, the amount of FCR in this specimen was lower than that in specimen CG (0.17%), which comprised only 0.17% of CNMs. This could be because of the higher sensitivity of the nanoscale conductive paths generated by the CNTs and GNPs compared to those generated by the microscale CFs. In general, an irreversible strain and FCR were observed at the end of each cycle (unloading), which can be attributed to the rearrangement of conductive fillers and/or micro-crack formation. However, the amount of residual strain and irreversible FCR in the fibre-reinforced specimens was lower than those of specimen CG (0.17%), which could be because of the ductility improvement of these specimens. To better evaluate the state of residual strain, the total strain of different reinforced specimens was measured at the end of each cycle by using the DIC method, as shown in Fig. 29.

As can be seen, specimen CG (0.17%) exhibits a high residual strain at the end of the third cycle, which can be because of the low ductility of this specimen. As shown in Fig. 29 (b) and (c), reinforcing this specimen with CFs decreased the residual strain and critical areas in terms of microcracks such that specimen CGC (0.75%) exhibited a lower total residual strain compared with the others. However, the excessive increase in CF concentration (up to 1.0%) in the specimen containing CNMs resulted in a higher residual strain than that of specimen CG (0.17%). Specimen CF (0.75%) which comprised only 0.75% CFs,

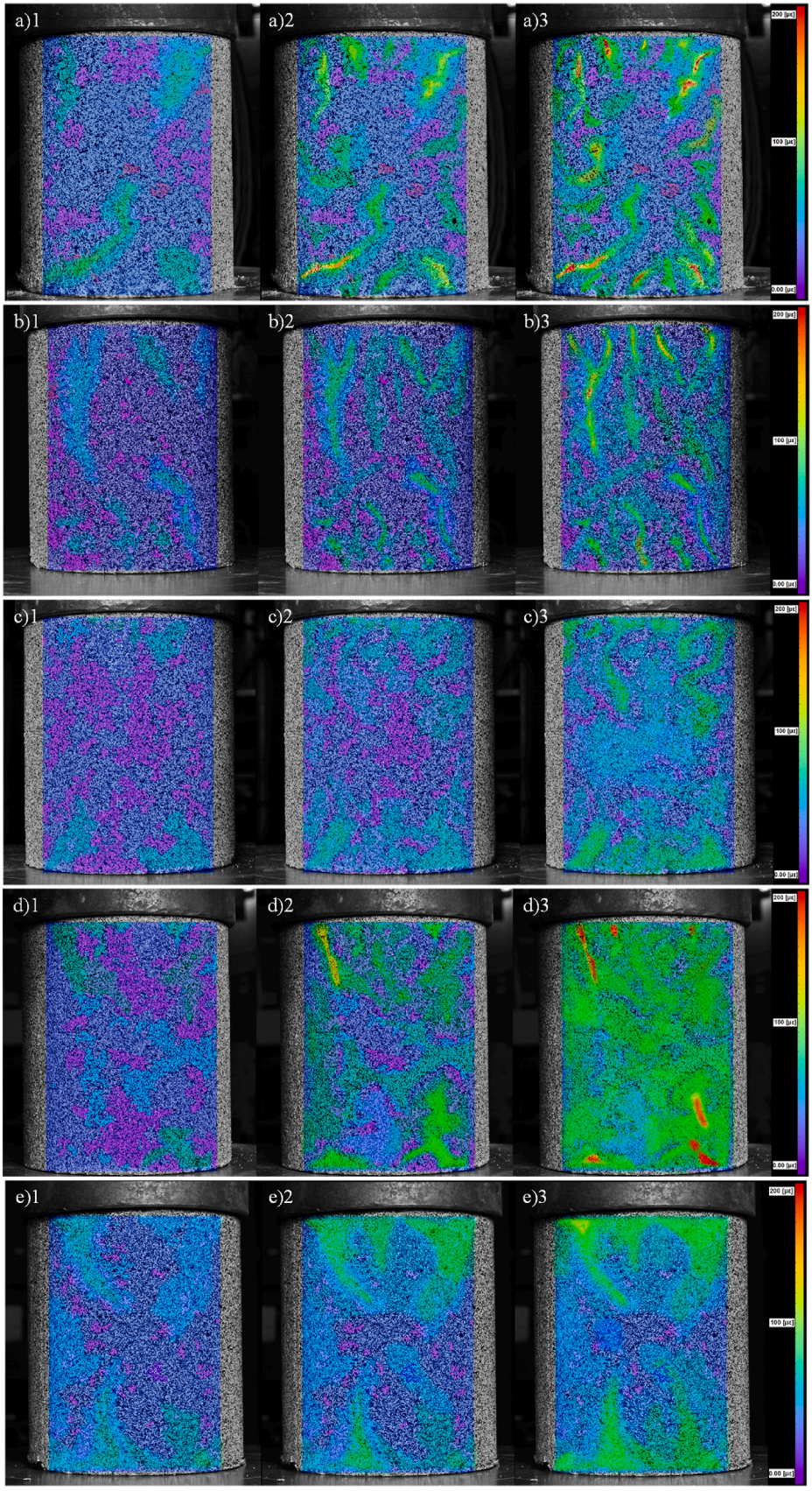

Fig. 29. Total strain of different reinforced CSS specimens: a) CG (0.17%), b) CGC (0.5%), c) CGC (0.75%), d) CGC (1.0%), and e) CF (0.75%) (Numbers represent the number of cycles.).

exhibited a lower residual strain compared with specimen CG (0.17%). However, the amount of FCR in this specimen was lower than that in CG (0.17%).

The above results, which are consistent with the outcomes discussed in the previous section, show the advantages of multiscale reinforcement in sustainability and piezoresistivity improvement of cementitious geocomposites. The ductility improvement of cementitious geocomposites is one of the most important aspects which can guarantee its sustainability and long-term operation in terms of mechanical performance and sensitivity, especially in the case of dynamic and traffic loads.

To better investigate the relationship between FCR and strain under cyclic compressive loading, the variation of FCR together with the axial strain for different reinforced CSS specimens is shown in Fig. 30.

Generally, power functions have been found to better express the relationship between the FCR and strain, based on a lower coefficient of determination (R^2).

The slope in the relationship between the strain and FCR represents the sensitivity of the composites as sensors for measuring compressive strain.

As can be seen, specimens CF (1.0%) and CG (0.17%) demonstrated higher data scatter and lower slope, respectively. In contrast, lower values of R^2 and a higher slope were exhibited by CGC (0.75%) and CGC (0.5%), respectively.

3.7.3. Gauge factors

The gauge factor for reinforced composites in different modes under cyclic compressive loads is shown in Fig. 31. As can be seen, the addition of 0.5% CFs to specimen CG (0.17%) which contained 0.17% of CNMs, increased the gauge factor of this specimen by approximately 86%. The gauge factors of specimens CGC (0.75%) and CGC (1.0%) were approximately 135% and 97% higher than that of CG (0.17%). However, the gauge factor of specimen CF (0.75%) which comprised only 0.75% of CF, was approximately 48% lower than that of specimen CG (0.17%).

As can be seen, the gauge factor is heavily dependent on the type of filler and its concentration. The types and concentrations of the conductive fillers have a significant impact on the amount, shape, and scale of the generated conductive paths. In addition, they can change the microstructure, and consequently, the physical and mechanical properties of the holder matrix, which can create changes in the gauge factor.

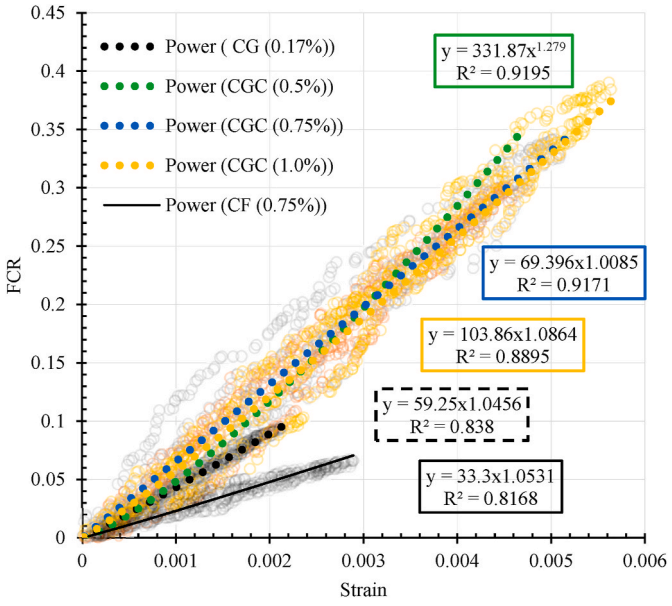

Fig. 30. Relationship between the FCR and strain for different reinforced CSS specimens.

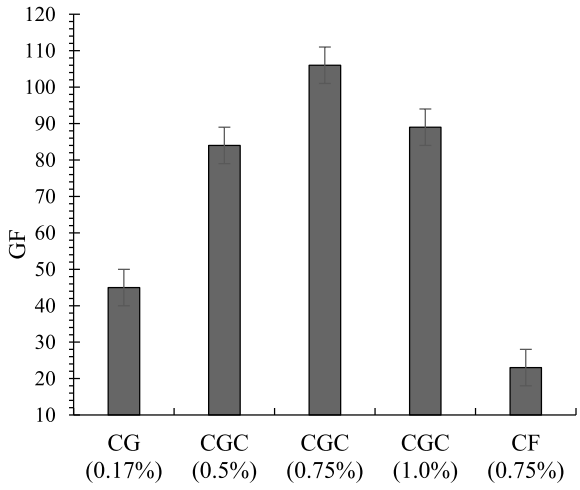

Fig. 31. Gauge factor for different reinforced CSS specimens.

Furthermore, the type of loading protocol is one of the most important factors in the variation of the obtained gauge factor.

Incorporation of a certain amount of CNTs and GNPs into the cementitious composite generally resulted in an increased sensitivity because of the nanoscale conductive paths that are very sensitive to small strains. However, the formation of these nanoscale paths in stiff composites with low ductility can cause noise. In addition, the efficiency of the composite as a sensor might be reduced after several loading cycles owing to microcrack formation. The presence of carbon microfibers not only increases the number of conductive networks and connects conductive regions formed by ions and CNMs, but also increases the ductility of the matrix, which can increase the gauge factor. However, the microscale conductive paths formed by CFs at relatively low concentrations are not very sensitive to small strains and contribute to decreasing the gauge factor.

4. Conclusion

We conducted an extensive study on the effects of multiscale conductive fillers, including carbon nanotubes (CNTs), graphene nanoplatelets (GNPs), and carbon fibres (CFs), on the microstructure, mechanical properties, durability, and piezoresistivity of cementitious stabilised sand (CSS). Different concentrations of CFs (0.5, 0.75, and 1.0%, by weight of dry sand) were incorporated into the plain CSS, and the specimens contained an optimum concentration of the hybrid CNT/GNP (0.17%, 1:1). The specimens were fabricated at the optimum water content using the standard compaction method. The interfacial properties of the fibres and the microstructure, mechanical properties, durability, and piezoresistivity of the specimens in different reinforcement modes were investigated by performing several tests after 28 d of hydration, and the following conclusions were drawn:

4. Scanning electron microscopy (SEM), energy-dispersive X-ray spectroscopy (EDX), X-ray diffraction (XRD), and Fourier transform infrared (FTIR) analyses of the treated CFs indicated roughing and rippling in addition to the formation of different oxygen functional groups on the fibre surface, including (-OH), (–COO–), (-*O*-), and (-*C*–SO_3–), during chemical treatment.
5. Moreover, we found via chemical analysis that the oxygen functional groups on the surface of the carbon fibre can react with the cement hydration products to form CH and *C*–S–H gel, indicating that the interfacial adhesion between the treated CFs and cement matrix would be improved. Furthermore, the single fibre pullout test showed a significant enhancement in the chemical debonding energy, frictional bond strength, and bond strength of the

modified CF by approximately 10, 2, and 3 times, respectively, than those of raw CFs.

6. The incorporation of 0.75% CFs into the specimen containing 0.17% CNT/GNP increased the maximum dry density and degree of saturation of the specimen to more than those of specimens with hybrid CNT/GNP and the individual utilisation of CFs. However, an excessive increase in CF concentration decreased the maximum dry density and degree of saturation and increased the optimum water content.
7. The SEM images showed the high efficiency of the CNT/GNP/CF combination in terms of filling a wider range of porosities and bridging cracks at different scales.
8. Thermographic analyses showed that the presence of 0.17% hybrid CNT/GNP in CSS increased the amount of hydration products. Inclusion of CFs into the specimen containing CNT/GNP and increasing its concentration consistently reduced the amount and/or rate of formation of cement hydration products compared with those of the CSS specimen with only CNT/GNPs.
9. Specimen CGC (0.75%), which comprised 0.17% CNT/GNP and 0.75% CF, exhibited a significant improvement in unconfined compressive strength (UCS) by approximately 96% and decreased the elastic modulus ($E_{50\%\ (tang)}$) by approximately 16%.
10. Specimen CGC (0.75%) also showed a 61% improvement in the weight loss of plain CSS after 12 wet and drying cycles. In addition, this specimen exhibited a 71% reduction in the permeability coefficient compared with that of plain CSS.
11. Multiscale application of the conductive filler also resulted in a significant improvement in the electrical conductivity and piezoresistive behaviour of the CSS compared with those observed with hybrid CNT/GNP and the individual utilisation of CFs. Furthermore, digital image correlation results showed lesser affected areas for specimen CGC (0.75%) in terms of residual strain and possible microcracks.
12. Specimen CGC (0.75%) also exhibited the maximum gauge factors, which were approximately 1.3 and 3.6 times higher than those of the specimens that contained only CNT/GNP and CF, respectively.

In summary, the above outcomes indicate the high potential of multiscale reinforcement in terms of hydro-mechanical, microstructural, durability, and piezoresistivity enhancement in CSS. We believe that this novel approach contributes to the new era of smart composite materials in intelligent structures.

Author statement

Conceptualization, M.A., R.F. and A.G.C.; methodology, M.A., R.F. and A.G.C.; validation, M.A., R.F. and A.G.C.; formal analysis, M.A., R.F. and A.G.C.; investigation, M.A., R.F. and A.G.C.; resources, M.A., R.F. and A.G.C.; data curation, M.A., R.F. and A.G.C.; writing original draft preparation, M.A., R.F. and A.G.C.; writing review and editing, M.A., R.F. and A.G.C.; visualization, M.A., R.F. and A.G.C.; supervision, A.G.C. and R.F.; project administration, A.G.C. and R.F.; funding acquisition, A.G.C. and R.F. All authors have read and agreed to the published version of the manuscript.

Data availability statement

Requests for all types of data used to support the findings of this study, after the publication of this article, will be considered by the corresponding author, subject to obtaining permission from the owners.

Declaration of competing interest

The authors declare that they have no known competing financial interests or personal relationships that could have appeared to influence the work reported in this paper.

Acknowledgements

This work was supported by the European Commission-Shift2Rail Program under the project “IN2TRACK3, H2020–S2RJU-CFM-2020, S2R-CFMIP3- 01–2020”. Furthermore, it is partly financed by FCT/MCTES through national funds (PIDDAC) under the R&D Unit of the Institute for Sustainability and Innovation in Engineering Structures (ISISE), under reference nº. 101012456, as well as under the R&D Unit of the Centre for Textile Science and Technology (2C2T).

References

[1] Y.-X. Zang, W. Gong, H. Xie, B.-L. Liu, H.-L. Chen, Chemical sand stabilization: a review of material, mechanism, and problems, Environ. Technol. Rev. 4 (1) (2015) 119–132.
[2] S. Paria, P.K. Yuet, Solidification–stabilization of organic and inorganic contaminants using portland cement, Environ. Rev. 14 (4) (2006) 217–255.
[3] S. Rana, P. Subramani, R. Fangueiro, A.G Correia, A review on smart self-sensing composite materials for civil engineering applications, AIMS Mater. Sci. 3 (2) (2016) 357–379.
[4] R. He, H. Ma, R.B. Hafiz, C. Fu, X. Jin, J. He, Determining porosity and pore network connectivity of cement-based materials by a modified non-contact electrical resistivity measurement: experiment and theory, Mater. Des. 156 (2018) 82–92.
[5] A. D’Alessandro, M. Rallini, F. Ubertini, A.L. Materazzi, J.M. Kenny, Investigations on scalable fabrication procedures for self-sensing carbon nanotube cement-matrix composites for SHM applications, Cement Concr. Compos. 65 (2016) 200–213.
[6] O. Jinping, H. Baoguo, Piezoresistive cement-based strain sensors and self-sensing concrete components, J. Intell. Mater. Syst. Struct. 20 (3) (2008) 329–336.
[7] B. Han, X. Yu, J. Ou, Self-sensing Concrete in Smart Structures, Butterworth-Heinemann, 2014.
[8] M. Abedi, R. Fangueiro, A. Gomes Correia, Ultra-sensitive affordable cementitious composite with high mechanical and microstructural performances by hybrid CNT/GNP, Materials. 13 (16) (2020) 3484.
[9] B. Han, S. Ding, X. Yu, Intrinsic self-sensing concrete and structures: a review, Measurement. 59 (2015) 110–128.
[10] W. Dong, W. Li, Z. Tao, K. Wang, Piezoresistive properties of cement-based sensors: review and perspective, Construct. Build. Mater. 203 (2019) 146–163.
[11] Y. Liu, M. Wang, W. Wang, Electric induced curing of graphene/cement-based composites for structural strength formation in deep-freeze low temperature, Mater. Des. 160 (2018) 783–793.
[12] G. Yıldırım, O. Öztürk, A. Al-Dahawi, A. Afşın Ulu, M. Şahmaran, Self-sensing capability of engineered cementitious composites: effects of aging and loading conditions, Construct. Build. Mater. 231 (2020) 117132.
[13] S. Nayak, S. Das, Spatial damage sensing ability of metallic particulate-reinforced cementitious composites: insights from electrical resistance tomography, Mater. Des. 175 (2019) 107817.
[14] W. Dong, W. Li, L. Shen, D. Sheng, Piezoresistive behaviours of carbon black cement-based sensors with layer-distributed conductive rubber fibres, Mater. Des. 182 (2019) 108012.
[15] X. Yao, C. Luan, D. Zhang, L. Lan, J. Fu, Evaluation of carbon fiber-embedded 3D printed structures for strengthening and structural-health monitoring, Mater. Des. 114 (2017) 424–432.
[16] M. Jung, J. Park, S-g Hong, J. Moon, Electrically cured ultra-high performance concrete (UHPC) embedded with carbon nanotubes for field casting and crack sensing, Mater. Des. 196 (2020) 109127.
[17] B. Suryanto, W.J. McCarter, G. Starrs, G.V. Ludford-Jones, Electrochemical immittance spectroscopy applied to a hybrid PVA/steel fiber engineered cementitious composite, Mater. Des. 105 (2016) 179–189.
[18] G. Yıldırım, M.H. Sarwary, A. Al-Dahawi, O. Öztürk, Ö. Anıl, M. Şahmaran, Piezoresistive behavior of CF- and CNT-based reinforced concrete beams subjected to static flexural loading: shear failure investigation, Construct. Build. Mater. 168 (2018) 266–279.
[19] B.G. Han, B.Z. Han, J.P. Ou, Experimental study on use of nickel powder-filled Portland cement-based composite for fabrication of piezoresistive sensors with high sensitivity, Sensor Actuators A: Phys. 149 (1) (2009) 51–55.
[20] A. Al-Dahawi, O. Öztürk, F. Emami, G. Yıldırım, M. Şahmaran, Effect of mixing methods on the electrical properties of cementitious composites incorporating different carbon-based materials, Construct. Build. Mater. 104 (2016) 160–168.
[21] B. Han, L. Zhang, S. Sun, X. Yu, X. Dong, T. Wu, et al., Electrostatic self-assembled carbon nanotube/nano carbon black composite fillers reinforced cement-based materials with multifunctionality, Compos. Appl. Sci. Manuf. 79 (2015) 103–115.
[22] M.R. Irshidat, M.H. Al-Saleh, H. Almashagbeh, Effect of carbon nanotubes on strengthening of RC beams retrofitted with carbon fiber/epoxy composites, Mater. Des. 89 (2016) 225–234.
[23] Z. Chen, J.L.G. Lim, E.-H. Yang, Ultra high performance cement-based composites incorporating low dosage of plasma synthesized carbon nanotubes, Mater. Des. 108 (2016) 479–487.

[24] S. Lv, Y. Ma, C. Qiu, T. Sun, J. Liu, Q. Zhou, Effect of graphene oxide nanosheets of microstructure and mechanical properties of cement composites, Construct. Build. Mater. 49 (2013) 121–127.

[25] G. Li, J.B. Yuan, Y.H. Zhang, N. Zhang, K.M. Liew, Microstructure and mechanical performance of graphene reinforced cementitious composites, Compos. Appl. Sci. Manuf. 114 (2018) 188–195.

[26] A. Akbar, K.M. Liew, Influence of elevated temperature on the microstructure and mechanical performance of cement composites reinforced with recycled carbon fibers, Compos. B Eng. 198 (2020) 108245.

[27] Z. Lu, A. Hanif, C. Ning, H. Shao, R. Yin, Z. Li, Steric stabilization of graphene oxide in alkaline cementitious solutions: mechanical enhancement of cement composite, Mater. Des. 127 (2017) 154–161.

[28] H.B. Birgin, A. D'Alessandro, S. Laflamme, F. Ubertini, Hybrid carbon microfibers-graphite fillers for piezoresistive cementitious composites, Sensors. 21 (2) (2021) 518.

[29] S.-J. Lee, I. You, G. Zi, D.-Y.J.S. Yoo, Experimental investigation of the piezoresistive properties of cement composites with hybrid carbon fibers and nanotubes, Sensors. 17 (11) (2017) 2516.

[30] S. Ding, Y. Ruan, X. Yu, B. Han, Y.-Q.J.C. Ni, B. Materials, Self-monitoring of smart concrete column incorporating CNT/NCB composite fillers modified cementitious sensors, Construct. Build. Mater. 201 (2019) 127–137.

[31] M. Sarwary, G. Yıldırım, A. Al-Dahawi, Ö. Anıl, KA. Khiavi, K. Toklu, et al., Self-sensing of flexural damage in large-scale steel-reinforced mortar beams, ACI Mater. J. 116 (4) (2019) 209–221.

[32] J. Han, J. Pan, J. Cai, X. Li, A review on carbon-based self-sensing cementitious composites, Construct. Build. Mater. 265 (2020) 120764.

[33] A. Al-Dahawi, G. Yıldırım, O. Öztürk, M. Şahmaran, Assessment of self-sensing capability of Engineered Cementitious Composites within the elastic and plastic ranges of cyclic flexural loading, Construct. Build. Mater. 145 (2017) 1–10.

[34] A. Khajeh, R. Jamshidi Chenari, M. Payan, A simple review of cemented non-conventional materials: soil composites, Geotech. Geol. Eng. 38 (2) (2020) 1019–1040.

[35] Z. Peng, X. Wang, Z. Wu, A bundle-based shear-lag model for tensile failure prediction of unidirectional fiber-reinforced polymer composites, Mater. Des. 196 (2020) 109103.

[36] B. Salazar, P. Aghdasi, I.D. Williams, C.P. Ostertag, H.K. Taylor, Polymer lattice-reinforcement for enhancing ductility of concrete, Mater. Des. 196 (2020) 109184.

[37] R.K.A. Al-Rub, B.M. Tyson, A. Yazdanbakhsh, Z. Grasley, Mechanical properties of nanocomposite cement incorporating surface-treated and untreated carbon nanotubes and carbon nanofibers, J. Nanomech. Micromech. 2 (1) (2012) 1–6.

[38] A. Lushnikova, A. Zaoui, Influence of single-walled carbon nantotubes structure and density on the ductility of cement paste, Construct. Build. Mater. 172 (2018) 86–97.

[39] M. Abedi, R. Fangueiro, A. Gomes Correia, Innovative self-sensing fiber-reinforced cemented sand with hybrid CNT/GNP, Smart Mater. Struct. (2021), https://doi.org/10.1088/1361-665X/ac2108. In press.

[40] M. Abedi, R. Fangueiro, A.G. Correia, An effective method for hybrid CNT/GNP dispersion and its effects on the mechanical, microstructural, thermal, and electrical properties of multifunctional cementitious composites, J. Nanomater. (2020) 6749150, 2020.

[41] M. Abedi, R. Fangueiro, A. Camões, A. Gomes Correia, Evaluation of CNT/GNP's synergic effects on the Mechanical, Microstructural, and durability properties of a cementitious composite by the novel dispersion method, Construct. Build. Mater. 260 (2020) 120486.

[42] M. Abedi, R. Fangueiro, A.G. Correia, Development of a novel multifunctional cementitious-based geocomposite by the contribution of CNT and GNP, Nanomaterials 11 (4) (2021) 961.

[43] S. Parveen, S. Rana, R. Fangueiro, M.C. Paiva, Characterizing dispersion and long term stability of concentrated carbon nanotube aqueous suspensions for fabricating ductile cementitious composites, Powder Technol. 307 (2017) 1–9.

[44] S. Parveen, S. Rana, R. Fangueiro, M.C. Paiva, Microstructure and mechanical properties of carbon nanotube reinforced cementitious composites developed using a novel dispersion technique, Cement Concr. Res. 73 (2015) 215–227.

[45] S. Alrekabi, A.B. Cundy, A. Lampropoulos, R.L.D. Whitby, I. Savina, Effect of high-intensity sonication on the dispersion of carbon-based nanofilaments in cementitious composites, and its impact on mechanical performance, Mater. Des. 136 (2017) 223–237.

[46] Q. Zhang, J. Wu, L. Gao, T. Liu, W. Zhong, G. Sui, et al., Dispersion stability of functionalized MWCNT in the epoxy–amine system and its effects on mechanical and interfacial properties of carbon fiber composites, Mater. Des. 94 (2016) 392–402.

[47] S. Parveen, S. Rana, R. Fangueiro, A review on nanomaterial dispersion, microstructure, and mechanical properties of carbon nanotube and nanofiber reinforced cementitious composites, J. Nanomater. (2013) 710175, 2013.

[48] H. Yu, S. Hermann, S.E. Schulz, T. Gessner, Z. Dong, W.J. Li, Optimizing sonication parameters for dispersion of single-walled carbon nanotubes, Chem. Phys. 408 (2012) 11–16.

[49] Z. Baig, O. Mamat, M. Mustapha, A. Mumtaz, K.S. Munir, M. Sarfraz, Investigation of tip sonication effects on structural quality of graphene nanoplatelets (GNPs) for superior solvent dispersion, Ultrason. Sonochem. 45 (2018) 133–149.

[50] B. Han, E. Guo, X. Xue, Z. Zhao, T. Li, Y. Xu, et al., Enhancement of the twisted carbon nanotube fibers properties by drawing processing and acid treatment, Mater. Des. 143 (2018) 238–247.

[51] A. Peled, H. Guttman, A. Bentur, Treatments of polypropylene fibres to optimize their reinforcing efficiency in cement composites, Cement Concr. Compos. 14 (4) (1992) 277–285.

[52] Compositions for preparing cement-adhesive reinforcing fibres, J.J. McAlpin, W. Y. Chow, Exxon chemical patents inc., linden, NJ, USA) US pat 4 861 812 (29 august 1989, Compos. Manuf. 1 (4) (1990) 265.

[53] B. Mobasher, V. Dey, J. Bauchmoyer, H. Mehere, S. Schaef, Reinforcing efficiency of micro and macro continuous polypropylene fibers in cementitious composites, Appl. Sci. 9 (2019) 2189.

[54] X. Wei, T. Ku, New design chart for geotechnical ground improvement: characterizing cement-stabilized sand, Acta Geotechnica. 15 (4) (2020) 999–1011.

[55] G. Vinoth, S.-W. Moon, J. Moon, T. Ku, Early strength development in cement-treated sand using low-carbon rapid-hardening cements, Soils Found. 58 (5) (2018) 1200–1211.

[56] L. Wang, F. Aslani, Development of self-sensing cementitious composites incorporating CNF and hybrid CNF/CF, Construct. Build. Mater. (2020) 121659.

[57] M. Safiuddin, M. Yakhlaf, K.A. Soudki, Key mechanical properties and microstructure of carbon fibre reinforced self-consolidating concrete, Construct. Build. Mater. 164 (2018) 477–488.

[59] A. Katz, VcJJomsl Li, A special technique for determining the bond strength of micro-fibres in cement matrix by pullout test, J. Mater. Sci. Lett. 15 (20) (1996) 1821–1823.

[60] M. Lu, H. Xiao, M. Liu, X. Li, H. Li, L. Sun, Improved interfacial strength of SiO2 coated carbon fiber in cement matrix, Cement Concr. Compos. 91 (2018) 21–28.

[61] A. Katz, C. Li Vcjmopla, Bond Properties of Micro-fibers in Cementitious Matrix 370, Cambridge University Press, 1994, p. 370.

[62] Z. Lin, T. Kanda, V.C. Li, On Interface Property Characterization and Performance of Fiber Reinforced Cementitious Composites, Concr. Sci. Eng. 1 (1999) 173–174.

[63] A. Peled, E. Zaguri, G. Marom, Bonding characteristics of multifilament polymer yarns and cement matrices, Compos. Appl. Sci. Manuf. 39 (6) (2008) 930–939.

[64] Y. Yilmaz, V. Ozaydin, Compaction and shear strength characteristics of colemanite ore waste modified active belite cement stabilized high plasticity soils, Eng. Geol. 155 (2013) 45–53.

[65] Y. Yilmaz, Experimental investigation of the strength properties of sand–clay mixtures reinforced with randomly distributed discrete polypropylene fibers, Geosynth. Int. 16 (5) (2009) 354–363.

[66] A.G. Correia, T. Valente, J. Tinoco, J. Falcão, J. Barata, D. Cebola (Eds.), Evaluation of Mechanical Properties of Jet Grouting Columns Using Different Test Methods. 17th International Conference on Soil Mechanics and Geotechnical Engineering (17th ICSMGE), IOS Press Alexandria, Egypt, 2009, pp. 2179–2171.

[67] P. Mohamed Shameer, P. Mohamed Nishath, Chapter 8 - exploration and enhancement on fuel stability of biodiesel: a step forward in the track of global commercialization, in: A.K. Azad, M. Rasul (Eds.), Advanced Biofuels, Woodhead Publishing, 2019, pp. 181–213.

[68] D. Titus, E. James Jebaseelan Samuel, S.M. Roopan, Chapter 12 - nanoparticle characterization techniques, in: A.K. Shukla, S. Iravani (Eds.), Green Synthesis, Characterization and Applications of Nanoparticles, Elsevier, 2019, pp. 303–319.

[69] S. Tiwari, J. Bijwe, Surface treatment of carbon fibers-a review, Procedia Technol. 14 (2014) 505–512.

[70] X. Fu, W. Lu, D.D.L. Chung, Improving the bond strength between carbon fiber and cement by fiber surface treatment and polymer addition to cement mix, Cement Concr. Res. 26 (7) (1996) 1007–1012.

[71] L. Lavagna, S. Musso, G. Ferro, M. Pavese, Cement-based composites containing functionalized carbon fibers, Cement Concr. Compos. 88 (2018) 165–171.

[72] H-j Fu, N-h Kuang, S-l Luan, Interfacial properties modification of carbon fiber/polyarylacetylene composites, Chin. J. Aeronaut. 20 (2) (2007) 124–128.

[73] F. Tatsuoka, A.G. Correia, Importance of controlling the degree of saturation in soil compaction, Procedia Engineering 143 (2016) 556–565.

[74] Z. Lafhaj, M. Goueygou, A. Djerbi, M. Kaczmarek, Correlation between porosity, permeability and ultrasonic parameters of mortar with variable water/cement ratio and water content, Cement Concr. Res. 36 (4) (2006) 625–633.

[75] B. Han, L. Zhang, C. Zhang, Y. Wang, X. Yu, J. Ou, Reinforcement effect and mechanism of carbon fibers to mechanical and electrically conductive properties of cement-based materials, Construct. Build. Mater. 125 (2016) 479–489.

[76] X. Cui, B. Han, Q. Zheng, X. Yu, S. Dong, L. Zhang, et al., Mechanical properties and reinforcing mechanisms of cementitious composites with different types of multiwalled carbon nanotubes, Compos. Appl. Sci. Manuf. 103 (2017) 131–147.

[77] J. Sun, F. Zhao, Y. Yao, X. Liu, Z. Jin, Y. Huang, A two-step method for high efficient and continuous carbon fiber treatment with enhanced fiber strength and interfacial adhesion, Mater. Lett. 196 (2017) 46–49.

[78] G.-H. Heo, J.-G. Park, K.-C. Song, J.-H. Park, H.-M. Jun, Improving the interfacial bond properties of the carbon fiber coated with a nano-SiO_2 particle in a cement paste matrix, Adv. Civ. Eng. (2020) 8838179, 2020.

[79] M.A. Trezza, Hydration study of ordinary portland cement in the presence of zinc ions, Mater. Res. 10 (2007) 331–334.

[80] C. Redon, V.C. Li, C. Wu, H. Hoshiro, T. Saito, A. Ogawa, Measuring and modifying interface properties of PVA fibers in ECC matrix, J. Mater. Civ. Eng. 13 (6) (2001) 399–406.

[81] S.M. Hejazi, M. Sheikhzadeh, S.M. Abtahi, A. Zadhoush, A simple review of soil reinforcement by using natural and synthetic fibers, Construct. Build. Mater. 30 (2012) 100–116.

[82] M.K. Gupta, R.K. Srivastava, Mechanical properties of hybrid fibers-reinforced polymer composite: a review, Polym. Plast. Technol. Eng. 55 (6) (2016) 626–642.

[83] S. Chakraborty, S.P. Kundu, A. Roy, B. Adhikari, S.B. Majumder, Effect of jute as fiber reinforcement controlling the hydration characteristics of cement matrix, Ind. Eng. Chem. Res. 52 (3) (2013) 1252–1260.

[84] E. Ganjian, H.S. Pouya, Effect of magnesium and sulfate ions on durability of silica fume blended mixes exposed to the seawater tidal zone, Cement Concr. Res. 35 (7) (2005) 1332–1343.

[85] L.P. Singh, A. Goel, S.K. Bhattacharyya, G. Mishra, Quantification of hydration products in cementitious materials incorporating silica nanoparticles, Front. Struct. Civ. Eng. 10 (2) (2016) 162–167.
[86] D. Shuang, W. Baomin, Study on dispersion of graphene nanoplates and rheological properties, early hydration of cement composites, Mater. Res. Express 6 (9) (2019), 095086.
[87] Y.-H. Chen, S.-C. Lin, J.-A. Wang, S.-Y. Hsu, C.-C.M. Ma, Preparation and properties of graphene/carbon nanotube hybrid reinforced mortar composites, Mag. Concr. Res. 71 (8) (2019) 395–407.
[88] B. Han, L. Zhang, S. Zeng, S. Dong, X. Yu, R. Yang, et al., Nano-core effect in nano-engineered cementitious composites, Compos. Appl. Sci. Manuf. 95 (2017) 100–109.
[89] B. Han, Q. Zheng, S. Sun, S. Dong, L. Zhang, X. Yu, et al., Enhancing mechanisms of multi-layer graphenes to cementitious composites, Compos. Appl. Sci. Manuf. 101 (2017) 143–150.
[90] T.S. Amhadi, G.J. Assaf, Strength and permeability potentials of cement-modified desert sand for roads construction purpose, Innovat. Infrastruct. Solut. 5 (3) (2020) 1–10.
[91] N.C. Consoli, D. Winter, H.B. Leon, H.C. Scheuermann, Engineering G. Durability, strength, and stiffness of green stabilized sand, J. Geotech. Geoenviron. Eng. 144 (9) (2018) 4018057.
[92] O.E. Ozbulut, Z. Jiang, D.K. Harris, Exploring scalable fabrication of self-sensing cementitious composites with graphene nanoplatelets, Smart Mater. Struct. 27 (11) (2018) 115029.
[93] O. Galao, F.J. Baeza, E. Zornoza, P. Garcés, Strain and damage sensing properties on multifunctional cement composites with CNF admixture, Cement Concr. Compos. 46 (2014) 90–98.
[94] C. Liu, G. Liu, Z. Ge, Y. Guan, Z. Cui, J. Zhou, Mechanical and self-sensing properties of multiwalled carbon nanotube-reinforced ECCs, Adv. Mater. Sci. Eng. (2019) 9..
[95] I. Rhee, J.S. Lee, Y.A. Kim, J.H. Kim, J.H. Kim, Electrically conductive cement mortar: incorporating rice husk-derived high-surface-area graphene, Construct. Build. Mater. 125 (2016) 632–642.
[96] A.O. Monteiro, P.B. Cachim, P.M. Costa, Self-sensing piezoresistive cement composite loaded with carbon black particles, Cement Concr. Compos. 81 (2017) 59–65.
[97] J.-L. Le, H. Du, S.D. Pang, Use of 2D Graphene Nanoplatelets (GNP) in cement composites for structural health evaluation, Compos. B Eng. 67 (2014) 555–563.
[98] J. Donnini, T. Bellezze, V. Corinaldesi, Mechanical, electrical and self-sensing properties of cementitious mortars containing short carbon fibers, Journal of Building Engineering 20 (2018) 8–14.
[99] S. Wen, D. Chung, Uniaxial compression in carbon fiber-reinforced cement, sensed by electrical resistivity measurement in longitudinal and transverse directions, Cement Concr. Res. 31 (2) (2001) 297–301.